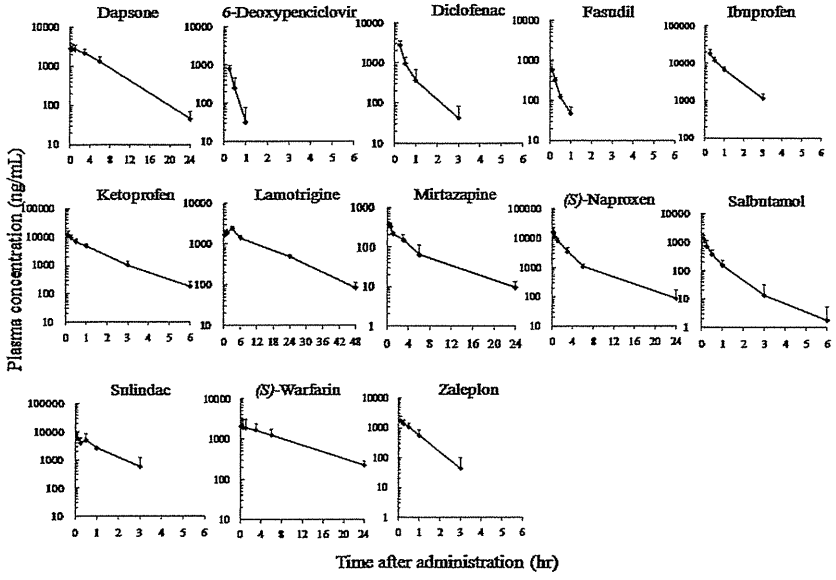

FIG. 2. Plasma concentrations after intravenous administration to PXB mice. Each point represents the mean ± S.D. (n = 3–5).

6-deoxypenciclovir, fasudil, sulindac, and zaleplon, were added in this study. These were reflected in the data set that spanned a wide range of PK parameter characteristics. CL_t and $t_{1/2}$ after intravenous administration of selected model drugs to humans were obtained from the literature. If CL_t after intravenous administration was not available from the literature, we used the value of CL_t/F after oral administration. The PK parameters and the major enzymes responsible for drug metabolism in humans are shown in Table 1. The spreadsheet containing these values with the literature references is included as an attachment in the supplemental data (Supplemental Tables 1 and 2).

Disappearance of Parent Drugs after Incubation. Remaining amounts of all of the compounds decreased linearly for 2 h on incubation with h-hepatocytes. The values of $CL_{int,in\ vitro}$ in hepatocytes, calculated using scaling factors to humans and PXB mice whole body as described under *Materials and Methods*, are listed in Table 2. These $CL_{int,in\ vitro}$ values covered a wide range. Fasudil showed high clearance, whereas warfarin was very stable.

PK Study of the Model Compounds in PXB Mice. Plasma concentrations and PK parameters in PXB mice after intravenous administration of drug solutions at 0.3 to 5 mg/kg are shown in Fig. 2 and Tables 3 and 4. Each RI value in PXB mice was 73.4 to 93.4%.

CL_t values of warfarin and lamotrigine were relatively low, whereas those of fasudil and salbutamol were much higher; the range of CL_t was 0.2 to 198 ml · min^{-1} · kg^{-1}. The $t_{1/2}$ value of lamotrigine was the longest, and those of 6-deoxypenciclovir and fasudil were short, as shown in Table 3.

Comparison of Intrinsic CL between h-Hepatocytes and Humans. Direct comparison between $CL_{int,in\ vitro}$ from h-hepatocytes and $CL_{int,in\ vivo}$ calculated for a well stirred model in humans showed a moderate correlation (r^2 = 0.475, p = 0.009) (Fig. 3). For 2 of 13 (15%) compounds, observed $CL_{int,in\ vivo}$ was predicted within a 3-fold error from hepatocyte $CL_{int,\ in\ vitro}$. However, for 8 of 13 (62%) compounds, observed $CL_{int,in\ vivo}$ was predicted with a 3- to 10-fold error.

Figure 4 shows the relationship between $CL_{int,in\ vivo}$ and $CL_{int,in\ vitro}$ for PXB mice; again, the correlation was moderate (r^2 = 0.435, p =

TABLE 3

Experimental conditions and RI values in PXB mice used for PK study

Each compound was administered intravenously to PXB mice at 0.3 to 5 mg/kg body weight. The values of RI of PXB mice ranged from 73.4 to 93.4%. Each value represents the mean ± S.D. (n = 3–5).

Compounds	Dose	RI	CL_t	$t_{1/2}$
	mg/kg	*%*	*ml · min^{-1} · kg^{-1}*	*h*
Dapsone	3.0	77.4 ± 5.5	2.1 ± 0.5	4.5 ± 1.1
6-Deoxypenciclovir	3.0	93.4 ± 4.2	71.2 ± 13.0	0.1 ± 0.1
Diclofenac	3.0	76.4 ± 2.1	16.4 ± 4.3	0.6 ± 0.2
Fasudil	3.0	75.8 ± 1.3	198.1 ± 14.6	0.3 ± 0.1
Ibuprofen	5.0	73.4 ± 3.2	3.8 ± 1.0	0.7 ± 0.1
Ketoprofen	3.0	74.0 ± 1.1	3.3 ± 0.6	1.1 ± 0.1
Lamotrigine	3.0	77.1 ± 4.0	1.4 ± 0.2	10.1 ± 0.9
Mirtazapine	3.0	79.8 ± 1.7	30.4 ± 9.4	6.0 ± 1.4
(*S*)-Naproxen	5.0	82.2 ± 6.1	2.2 ± 0.5	4.8 ± 2.7
Salbutamol	3.0	74.5 ± 0.7	79.9 ± 34.0	0.6 ± 0.3
Sulindac	3.0	74.5 ± 2.0	5.6 ± 1.3	1.2 ± 0.8
(*S*)-Warfarin	0.3	75.3 ± 1.8	0.2 ± 0.1	8.2 ± 2.8
Zaleplon	3.0	77.1 ± 3.7	48.1 ± 7.1	0.7 ± 0.4

TABLE 4

$CL_{int,in\ vivo}$ of humans and PXB mice, calculated by a well stirred model

$CL_{int,in\ vivo}$ was calculated from in vivo CL_t, fu, Rb, and Q based on a well stirred model. The Q values of humans and PXB mice were set at 21 and 90 ml · min^{-1} · kg^{-1} (same as in normal mice), respectively. In addition, Rb and fu of human were assumed to be equivalent to those of PXB mice. If total CL of drugs exceeded liver blood flow, then the hepatic clearance was taken as 90% of liver blood flow. $CL_{int,in\ vivo}$ of 6-deoxypenciclovir, lamotrigine, and sulindac were evaluated from CL_{oral} as $CL_{oral}/fu/Rb$.

Compounds	Human $CL_{int,in\ vivo}$	PXB Mice $CL_{int,in\ vivo}$
	ml · min^{-1} · kg^{-1}	
Dapsone	2.0	8.6
6-Deoxypenciclovir	118.0	209.0
Diclofenac	1004.3	4905.1
Fasudil	370.6	1588.2
Ibuprofen	147.1	686.0
Ketoprofen	232.2	442.0
Lamotrigine	0.7	3.2
Mirtazapine	123.6	408.7
(*S*)-Naproxen	10.1	230.2
Salbutamol	13.5	1148.2
Sulindac	47.8	86.5
(*S*)-Warfarin	3.7	13.4
Zaleplon	173.6	261.3

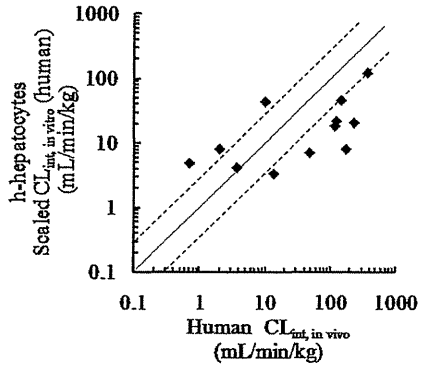

FIG. 3. Correlation between observed human $CL_{int,in\ vivo}$ and $CL_{int,in\ vitro}$ of PXB mouse hepatocytes, calculated as described in the text. The solid line represents unity. The dotted line represents the range within 3-fold of unity.

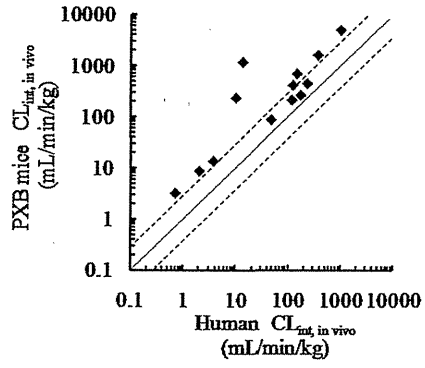

FIG. 5. Correlation of $CL_{int,in\ vivo}$ between humans and PXB mice, calculated as described in the text. The solid line represents unity. The dotted line represents the range within 3-fold of unity.

0.014). For 6 of 13 (46%) compounds, $CL_{int,in\ vivo}$ of PXB mice was predicted within a 3-fold error from h-hepatocyte $CL_{int,in\ vitro}$. For 5 of 13 (38%) compounds, $CL_{int,in\ vivo}$ was predicted within a 3- to 10-fold error.

Relationship between Intrinsic Clearance in Humans and PXB Mice In Vivo. We directly compared $CL_{int,in\ vivo}$ calculated based on a well stirred model in humans and PXB mice. As shown in Fig. 5, there was a good correlation ($r^2 = 0.754$, $p = 1.174 \times 10^{-4}$) between literature $CL_{int,in\ vivo}$ in human and measured $CL_{int,in\ vivo}$ of PXB mice for these compounds. For 4 of 13 (31%) compounds, observed $CL_{int\ in\ vivo}$ in humans was predicted within a 3-fold error from PXB mouse $CL_{int,in\ vivo}$. For 7 of 13 (54%) compounds, human $CL_{int,in\ vivo}$ was predicted within a 3- to 10-fold error.

Relationship of Elimination $t_{1/2}$ between Humans and PXB mice. Figure 6 shows the relationship of $t_{1/2}$ after intravenous administration between humans and PXB mice. Compounds for which literature data were not available were excluded from this figure. A good correlation ($r^2 = 0.886$, $p = 1.506 \times 10^{-4}$) was found. For 6 of 9 (67%) compounds, human observed $t_{1/2}$ was predicted within a 3-fold error from PXB mice $t_{1/2}$. For 3 of 9 (33%) compounds, the error was in the range of 3- to 10-fold.

Discussion

The prediction of human PK parameters is an important step during the preclinical development of pharmaceuticals to reduce costs by enabling the early elimination of candidates with unsuitable properties. However, species differences make it difficult to predict human PK from animal data; monkey data may lead to underprediction (Chiou and Buehler, 2002; Akabane et al., 2010), whereas dog data may cause overestimation (Chiou et al., 2000). In vitro-in vivo scaling from data obtained with human hepatic microsomes and hepatocytes is a widely used approach but often results in the underprediction of in vivo CL (Obach, 1999). We considered the possibility that PXB mice, in which hepatocytes are replaced with human hepatocytes to the extent of approximately 80% (Tateno et al., 2004), may have superior predictive utility, because the expression levels and activities of both P450 and non-P450 enzymes well reflect those of the donor hepatocytes (Yoshitsugu et al., 2006; Yamasaki et al., 2010). In this study, we checked metabolic activities (CYP2C9, CYP2D6, UGT, SULT, and AO) using probe substrates between donor hepatocytes and h-hepatocytes purified from PXB mice (Supplemental Table 3) as well as the expression of drug transporters and blood albumin (Tateno et al., 2004; Nishimura et al., 2005).

For the present study, we selected 13 model compounds with diverse chemical structures (Fig. 1), which are metabolized through multiple pathways by P450 and non-P450 enzymes, such as UGT, SULT, and AO. Their values of CL cover a wide range from 0.055 to 118 ml · min^{-1} · kg^{-1} (Table 1).

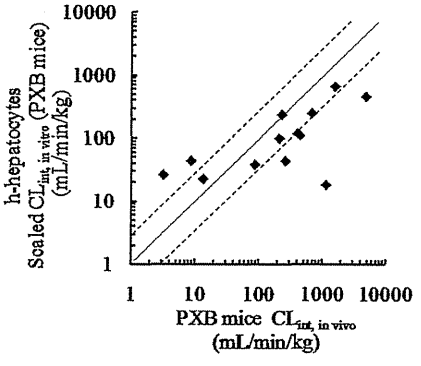

FIG. 4. Correlation between $CL_{int,in\ vivo}$ of PXB mice and $CL_{int,in\ vitro}$ of their hepatocytes, calculated as described in the text. The solid line represents unity. The dotted line represents the range within 3-fold of unity.

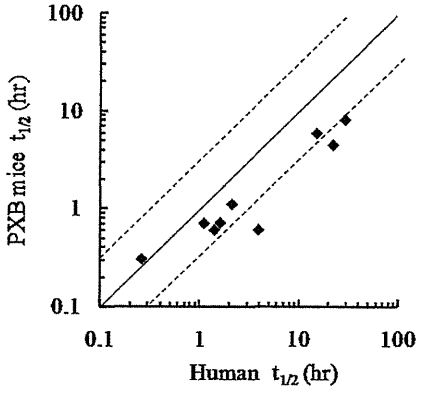

FIG. 6. Correlation of $t_{1/2}$ after intravenous administration between humans and PXB mice. Compounds for which literature data were not available were excluded from this figure. The solid line represents unity. The dotted line represents the range within 3-fold of unity.

First, we performed an in vitro metabolic study using fresh h-hepatocytes isolated from PXB mice. We calculated $CL_{int,in\ vitro}$ using fresh h-hepatocytes and compared the results with human $CL_{int,in\ vivo}$ estimated by use of a well stirred model (Pang and Rowland, 1977). These results using a parallel tube model and a dispersion model were also similar to those of a well stirred model (S. Sanoh, unpublished observations). A moderate correlation ($r^2 = 0.475$, $p = 0.009$) was found, but this approach was not superior to prediction using other methods.

$CL_{int,in\ vitro}$ values of diclofenac, ibuprofen, warfarin, and zaleplon were approximately similar to reported values using cryopreserved hepatocytes (Ekins and Obach, 2000; Nagilla et al., 2006; Stringer et al., 2008), supporting the idea that $CL_{int,in\ vitro}$ values are similar in fresh hepatocytes and cryopreserved hepatocytes (Naritomi et al., 2003; McGinnity et al., 2004).

A similar correlation ($r^2 = 0.435$, $p = 0.014$) was observed between $CL_{int,in\ vitro}$ and $CL_{int,in\ vivo}$ in PXB mice (Fig. 4). In both cases, the numbers of compounds for which absolute values of CL_{int} were predicted within a 3-fold error were insufficient.

Therefore, we next evaluated the predictability of hepatic clearance and $t_{1/2}$ from in vivo data in PXB mice. The values of $CL_{int,in\ vivo}$ estimated by intravenous administration in PXB mice were well correlated ($r^2 = 0.754$, $p = 1.174 \times 10^{-4}$) with observed $CL_{int,in\ vivo}$ in human. Surprisingly, we also found a good correlation ($r^2 = 0.886$, $p = 1.506 \times 10^{-4}$) between $t_{1/2}$ values in PXB mice and humans. However, although the rank order was the same, there were rather large prediction errors, so it may not be possible to predict absolute values. This is consistent with the findings of Xiao et al. (2010) in PXB mice.

We used PXB mice that showed that the average RI values were approximately 80%. It was a concern that the contribution of the remaining approximately 20% mice hepatocytes may be reflected on clearance. $CL_{int,in\ vitro}$ values of these model compounds in host mice hepatocytes (severe combined immunodeficiency mice) were almost higher than those of h-hepatocytes within a 10-fold range (Supplemental Fig. 1). The extent of the difference may not influence the predictability of $CL_{int,in\ vivo}$.

For the estimation of $CL_{int,in\ vivo}$ in PXB mice, the fu values of those model compounds is the same as those in humans because human albumin is expressed in the blood of PXB mice. Inoue et al. (2009) reported fu value of warfarin in PXB mice was similar to that in humans. Furthermore, fu values of some compounds (dapsone, diclofenac, ketoprofen, salbutamol, and zaleplon) in this study were also approximately similar to those in humans (S. Sanoh, unpublished observations).

We assumed that the Rb values of those model compounds is also the same as those in humans, because Rb values of some compounds (dapsone, diclofenac, ketoprofen, salbutamol, and zaleplon) in this study were also approximately similar to those in humans (S. Sanoh, unpublished observations).

Q values were assumed to be 90 $ml \cdot min^{-1} \cdot kg^{-1}$, respectively, corresponding to the values of normal mice (Davies and Morris, 1993). In further work, it would be desirable to examine whether these values are appropriate.

In this study, we selected model compounds metabolized not only by P450, but also by non-P450 enzymes, including AO. 6-Deoxypenciclovir, fasudil, sulindac, and zaleplon are metabolized mainly by AO in humans. It has been reported that human CL for drugs metabolized by AO may be underpredicted from data obtained with human liver cytosol and S9 due to the loss or deactivation of AO during preparation, homogenization, storage, and experimental procedures (Zientek et al., 2010). PXB mice have high AO activity, being similar to humans (Kitamura et al., 2008), and may be a useful source of fresh h-hepatocytes.

Our results indicate that PXB mice can be used at least for semi-quantitative prediction of not only CL_t but also $t_{1/2}$ in humans. PXB mice also would be useful for in vitro estimation and comparison of PK of various candidate compounds, because large amounts of fresh, identical hepatocytes (1.1×10^8 cells/mouse) are available by transplantation of donor hepatocytes (2.5×10^5 cells/mouse). The combination of in vitro study in PXB mice and in vitro study using PXB hepatocytes may prove to be particularly effective.

Acknowledgments

We thank members in PhoenixBio Co., Ltd. for the isolation of hepatocytes from PXB mice.

Authorship Contributions

Participated in research design: Sanoh, Sugihara, Kotake, Tayama, Horie, Kitamura, and Ohta.

Conducted experiments: Sanoh and Horiguchi.

Contributed new reagents or analytic tools: Sugihara, Ohshita, and Tateno.

Performed data analysis: Sanoh and Horiguchi.

Wrote or contributed to the writing of the manuscript: Sanoh, Kotake, Tateno, and Ohta.

References

Akabane T, Tabata K, Kadono K, Sakuda S, Terashita S, and Teramura T (2010) A comparison of pharmacokinetics between humans and monkeys. *Drug Metab Dispos* **38**:308–316.

Brown HS, Griffin M, and Houston JB (2007) Evaluation of cryopreserved human hepatocytes as an alternative in vitro system to microsomes for the prediction of metabolic clearance. *Drug Metab Dispos* **35**:293–301.

Chiba M, Ishii Y, and Sugiyama Y. (2009) Prediction of hepatic clearance in human from in vitro data for successful drug development. *AAPS J* **11**:262–276.

Chiou WL and Buehler PW (2002) Comparison of oral absorption and bioavailability of drugs between monkey and human. *Pharm Res* **19**:868–874.

Chiou WL, Jeong HY, Chung SM, and Wu TC (2000) Evaluation of using dog as an animal model to study the fraction of oral dose absorbed of 43 drugs in humans. *Pharm Res* **17**:135–140.

Davies B and Morris T (1993) Physiological parameters in laboratory animals and humans. *Pharm Res* **10**:1093–1095.

De Buck SS, Sinha VK, Fenu LA, Nijsen MJ, Mackie CE, and Gilissen RA (2007) Prediction of human pharmacokinetics using physiologically based modeling: a retrospective analysis of 26 clinically tested drugs. *Drug Metab Dispos* **35**:1766–1780.

De Serres M, Bowers G, Boyle G, Beaumont C, Castellino S, Sigafoos J, Dave M, Roberts A, Shah V, Olson K, et al. (2011) Evaluation of a chimeric (uPA+/+)/SCID mouse model with a humanized liver for prediction of human metabolism. *Xenobiotica* **41**:464–475.

Ekins S and Obach RS (2000) Three-dimensional quantitative structure activity relationship computational approaches for prediction of human in vitro intrinsic clearance. *J Pharmacol Exp Ther* **295**:463–473.

Fagerholm U (2007) Prediction of human pharmacokinetics–evaluation of methods for prediction of hepatic metabolic clearance. *J Pharm Pharmacol* **59**:803–828.

Hallifax D, Foster JA, and Houston JB (2010) Prediction of human metabolic clearance from in vitro systems: retrospective analysis and prospective view. *Pharm Res* **27**:2150–2161.

Huang L, Berry L, Ganga S, Janosky B, Chen A, Roberts J, Colletti AE, and Lin MH (2010) Relationship between passive permeability, efflux, and predictability of clearance from in vitro metabolic intrinsic clearance. *Drug Metab Dispos* **38**:223–231.

Inoue T, Sugihara K, Ohshita H, Horie T, Kitamura S, and Ohta S (2009) Prediction of human disposition toward S-3H-warfarin using chimeric mice with humanized liver. *Drug Metab Pharmacokinet* **24**:153–160.

Kamimura H, Nakada N, Suzuki K, Mera A, Souda K, Murakami Y, Tanaka K, Iwatsubo T, Kawamura A, and Usui T (2010) Assessment of chimeric mice with humanized liver as a tool for predicting circulating human metabolites. *Drug Metab Pharmacokinet* **25**:223–235.

Katoh M, Matsui T, Nakajima M, Tateno C, Kataoka M, Soeno Y, Horie T, Iwasaki K, Yoshizato K, and Yokoi T (2004) Expression of human cytochromes P450 in chimeric mice with humanized liver. *Drug Metab Dispos* **32**:1402–1410.

Katoh M, Matsui T, Okumura H, Nakajima M, Nishimura M, Naito S, Tateno C, Yoshizato K, and Yokoi T (2005) Expression of human phase II enzymes in chimeric mice with humanized liver. *Drug Metab Dispos* **33**:1333–1340.

Kitamura S, Nitta K, Tayama Y, Tanoue C, Sugihara K, Inoue T, Horie T, and Ohta S (2008) Aldehyde oxidase-catalyzed metabolism of N1-methylnicotinamide in vivo and in vitro in chimeric mice with humanized liver. *Drug Metab Dispos* **36**:1202–1205.

McGinnity DF, Soars MG, Urbanowicz RA, and Riley RJ (2004) Evaluation of fresh and cryopreserved hepatocytes as in vitro drug metabolism tools for the prediction of metabolic clearance. *Drug Metab Dispos* **32**:1247–1253.

Nagilla R, Frank KA, Jolivette LJ, and Ward KW (2006) Investigation of the utility of published in vitro intrinsic clearance data for prediction of in vivo clearance. *J Pharmacol Toxicol Methods* **53**:106–116.

Naritomi Y, Terashita S, Kagayama A, and Sugiyama Y (2003) Utility of hepatocytes in predicting drug metabolism: comparison of hepatic intrinsic clearance in rats and humans in vivo and in vitro. *Drug Metab Dispos* **31**:580–588.

Nishimura M, Yoshitsugu H, Yokoi T, Tateno C, Kataoka M, Horie T, Yoshizato K, and Naito

S (2005) Evaluation of mRNA expression of human drug-metabolizing enzymes and transporters in chimeric mouse with humanized liver. *Xenobiotica* **35**:877–890.

Obach RS (1999) Prediction of human clearance of twenty-nine drugs from hepatic microsomal intrinsic clearance data: An examination of in vitro half-life approach and nonspecific binding to microsomes. *Drug Metab Dispos* **27**:1350–1359.

Paixão P, Gouveia LF, and Morais JA (2010) Prediction of the in vitro intrinsic clearance determined in suspensions of human hepatocytes by using artificial neural networks. *Eur J Pharm Sci* **39**:310–321.

Pang KS and Rowland M (1977) Hepatic clearance of drugs. I. Theoretical considerations of a "well-stirred" model and a "parallel tube" model. Influence of hepatic blood flow, plasma and blood cell binding, and the hepatocellular enzymatic activity on hepatic drug clearance. *J Pharmacokinet Biopharm* **5**:625–653.

Stringer R, Nicklin PL, and Houston JB (2008) Reliability of human cryopreserved hepatocytes and liver microsomes as in vitro systems to predict metabolic clearance. *Xenobiotica* **38**:1313–1329.

Tabata K, Hamakawa N, Sanoh S, Terashita S, and Teramura T (2009) Exploratory population pharmacokinetics (e-PPK) analysis for predicting human PK using exploratory ADME data during early drug discovery research. *Eur J Drug Metab Pharmacokinet* **34**:117–128.

Tateno C, Yoshizane Y, Saito N, Kataoka M, Utoh R, Yamasaki C, Tachibana A, Soeno Y, Asahina K, Hino H, et al. (2004) Near completely humanized liver in mice shows human-type metabolic responses to drugs. *Am J Pathol* **165**:901–912.

Wang Q, Jia R, Ye C, Garcia M, Li J, and Hidalgo IJ (2005) Glucuronidation and sulfation of 7-hydroxycoumarin in liver matrices from human, dog, monkey, rat, and mouse. *In Vitro Cell Dev Biol Anim* **41**:97–103.

Xiao G, Bohnert T, Black C, Klunk L, and Gan LS (2010) Evaluation of chimeric mice with humanized liver to predict human intrinsic clearance of drug molecules at preclinical phase. *Drug Metab Rev* **42(S1:)**P60.

Yamasaki C, Kataoka M, Kato Y, Kakuni M, Usuda S, Ohzone Y, Matsuda S, Adachi Y, Ninomiya S, Itamoto T, et al. (2010) In vitro evaluation of cytochrome P450 and glucuronidation activities in hepatocytes isolated from liver-humanized mice. *Drug Metab Pharmacokinet* **25**:539–550.

Yamazaki H, Kuribayashi S, Inoue T, Tateno C, Nishikura Y, Oofusa K, Harada D, Naito S, Horie T, and Ohta S (2010) Approach for in vivo protein binding of 5-n-butyl-pyrazolo[1,5-a]pyrimidine bioactivated in chimeric mice with humanized liver by two-dimensional electrophoresis with accelerator mass spectrometry. *Chem Res Toxicol* **23**:152–158.

Yoshitsugu H, Nishimura M, Tateno C, Kataoka M, Takahashi E, Soeno Y, Yoshizato K, Yokoi T, and Naito S (2006) Evaluation of human CYP1A2 and CYP3A4 mRNA expression in hepatocytes from chimeric mice with humanized liver. *Drug Metab Pharmacokinet* **21**:465–474.

Zientek M, Jiang Y, Youdim K, and Obach RS (2010) In vitro-in vivo correlation for intrinsic clearance for drugs metabolized by human aldehyde oxidase. *Drug Metab Dispos* **38**:1322–1327.

Address correspondence to: Dr. Seigo Sanoh, Graduate School of Biomedical Sciences, Hiroshima University, Kasumi 1-2-3, Minami-ku, Hiroshima 734-8553 Japan. E-mail: sanoh@hiroshima-u.ac.jp

Cell Reports
Resource

Generation and Characterization of Severe Combined Immunodeficiency Rats

Tomoji Mashimo,[1,*] Akiko Takizawa,[1] Junya Kobayashi,[2] Yayoi Kunihiro,[1] Kazuto Yoshimi,[1] Saeko Ishida,[1] Koji Tanabe,[3] Ami Yanagi,[5] Asato Tachibana,[5] Jun Hirose,[4] Jun-ichiro Yomoda,[4] Shiho Morimoto,[1] Takashi Kuramoto,[1] Birger Voigt,[1] Takeshi Watanabe,[4] Hiroshi Hiai,[1] Chise Tateno,[5,6] Kenshi Komatsu,[2] and Tadao Serikawa[1]
[1]Institute of Laboratory Animals, Graduate School of Medicine
[2]Genome Repair Dynamics, Radiation Biology Center
[3]Department of Reprogramming Science, Center for iPS Cell Research and Application
[4]Center for Innovation in Immunoregulative Technology and Therapeutics, Graduate School of Medicine
Kyoto University, Kyoto 606-8501, Japan
[5]PhoenixBio. Co., Ltd., Higashihirosima, Hiroshima 739-0046, Japan
[6]Liver Research Project Center, Hiroshima University, Hiroshima 734-8551, Japan
*Correspondence: tmashimo@anim.med.kyoto-u.ac.jp
http://dx.doi.org/10.1016/j.celrep.2012.08.009

SUMMARY

Severe combined immunodeficiency (SCID) mice, the most widely used animal model of DNA-PKcs (*Prkdc*) deficiency, have contributed enormously to our understanding of immunodeficiency, lymphocyte development, and DNA-repair mechanisms, and they are ideal hosts for allogeneic and xenogeneic tissue transplantation. Here, we use zinc-finger nucleases to generate rats that lack either the *Prkdc* gene (SCID) or the *Prkdc* and *Il2rg* genes (referred to as F344-*scid gamma* [FSG] rats). SCID rats show several phenotypic differences from SCID mice, including growth retardation, premature senescence, and a more severe immunodeficiency without "leaky" phenotypes. Double-knockout FSG rats show an even more immunocompromised phenotype, such as the abolishment of natural killer cells. Finally, xenotransplantation of human induced pluripotent stem cells, ovarian cancer cells, and hepatocytes shows that SCID and FSG rats can act as hosts for xenogeneic tissue grafts and stem cell transplantation and may be useful for preclinical testing of new drugs.

INTRODUCTION

DNA-dependent protein kinase catalytic subunits (DNA-PKcs) are critical components of the nonhomologous end-joining (NHEJ) pathway of the DNA double-strand break (DSB) repair system. DSBs are usually generated by environmental influences such as ionizing radiation (IR) or by chemical mutagens, or are created during programmed processes such as V(D)J recombination or class switch recombination (CSR), which occur during lymphocyte development (Franco et al., 2006; Mahaney et al., 2009; Shrivastav et al., 2008; Yan et al., 2007). The Ku70/80 heterodimer first binds to the ends of the DSBs and recruits DNA-PKcs to form the active DNA-PK complex. Subsequently, together with Artimis, DNA-PKcs stimulate the processing of the DNA ends. Finally, the LIG4 complex, comprising LIG4, XRCC4, and XLF, seals the DSBs generated during NHEJ. Humans and several types of mammals with a defect in the genes involved in NHEJ cannot complete V(D)J recombination. This blocks lymphocyte development, resulting in severe combined immunodeficiency (SCID) (Bosma et al., 1983; O'Driscoll and Jeggo, 2006; Perryman, 2004; van der Burg et al., 2009). SCID mice, which arose spontaneously due to the defective DNA-PKcs gene (*Prkdc*), show an immunodeficient phenotype and increased sensitivity to IR (Bosma et al., 1983). In contrast, no *PRKDC* mutations had been reported in humans until recently, when a hypomorphic mutation with *PRKDC* kinase activity was identified in a patient with SCID with sensitivity to IR (RS-SCID; van der Burg et al., 2009). Although complete *PRKDC* deficiency is expected to be lethal in humans, spontaneous null mutations in the *PRKDC* gene were reported in Arabian horses and Jack Russell terriers, highlighting the fact that *PRKDC* deficiency is not tolerated equally in all species (Perryman, 2004).

SCID animals are widely used in biomedical research as hosts for allogeneic and xenogeneic tissue grafts. Humanized mice (i.e., immunodeficient mice engrafted with human cells or tissues, such as human hematopoietic stem cells [hHSCs], hepatocytes, or tumor cells) are powerful tools that have enabled scientists to gain greater insights into many human diseases (Azuma et al., 2007; Baiocchi et al., 2010; Brehm et al., 2010; Denton and García, 2011; Ito et al., 2008; Katoh et al., 2008; Kneteman and Mercer, 2005; Leonard, 2001; Meuleman et al., 2005; Pearson et al., 2008; Quintana et al., 2008; Shultz et al., 2007; Wege et al., 2008). Although the laboratory rat is an ideal model for physiological, pharmacological, toxicological, and transplantation studies, there are no reports of spontaneous, or gene-targeted, SCID rats. Recently, several strategies have been developed to produce a wide variety of genomic alterations in rats (Geurts et al., 2009; Izsvák et al., 2010; Mashimo et al., 2008; Tesson et al., 2011), including embryonic-stem-cell-derived p53 knockout rats (Tong et al., 2010). Other investigators

Cell PRESS
Open ACCESS

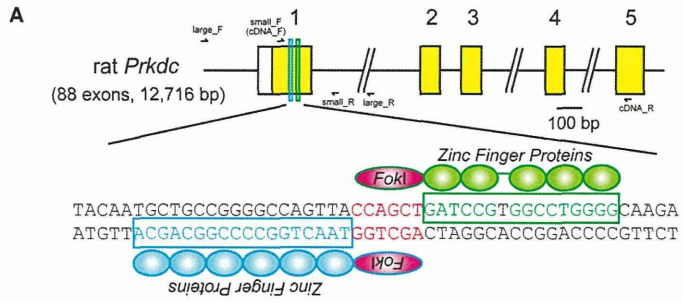

B

Strain	Targeted gene	Injected oocytes	Survived embryos	Transferred oocytes (%)	Born (%)	Mutants (%)
F344/Stm	*Prkdc*	148	115 (77.7)	107 (72.3)	♂6, ♀10 (12.1)	♂3, ♀1 (25.0)
Crlj:WI	*Prkdc*	215	163 (75.8)	133 (61.9)	♂16, ♀7 (17.3)	♂15, ♀7 (95.7)
F344/Stm	*Prkdc* & *Il2rg*	219	128 (58.4)	85 (38.8)	♂6, ♀8 (16.5)	♂1, ♀1*(14.8)

*Double injection of *Prkdc* and *Il2rg* ZFN-encoding mRNA provided one female carrying mutations in both *Prkdc* and *Il2rg* genes.

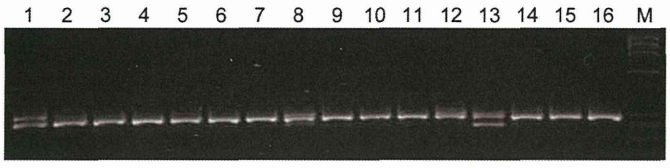

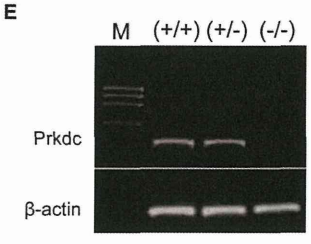

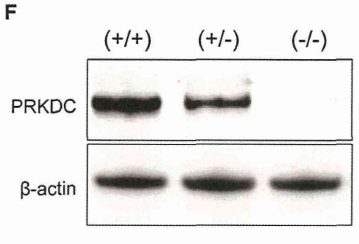

Figure 1. Injection of ZFN-Encoding mRNA into Rat Embryos Induces Targeted Loss-of-Function Mutations

(A) Schematic representation of the part of rat *Prkdc* gene. The magnified views illustrate the binding sites for the ZFN pairs.

(B) Injection of ZFN-encoding mRNA into F344/Stm or Crlj:WI rat fertilized oocytes.

(C) PCR analysis of 16 offspring obtained by ZFN injection of F344/Stm oocytes. M, DNA molecular weight marker φX174-HaeIII digest.

(D) Sequencing assay for ZFN-induced mutations in the target region in F344 rats. Multiple deletions and insertions are depicted by red dashes and letters, respectively, and are aligned along the WT sequences shown on the top line.

(E) RT-PCR analysis of *Prkdc* mRNA expression in the spleen of *Prkdc* (+/+, +/−, −/−) rats. *Gapdh* mRNA expression was used as an internal control.

(F) Western blot of PRKDC protein in the spleen of *Prkdc* (+/+, +/−, −/−) rats. β-actin was used as a loading control.

See also Figures S1 and S4.

and our group have also shown the successful application of zinc-finger nucleases (ZFNs) as a gene-targeting technology in rats, which is faster and more efficient than embryonic-stem-cell-mediated knockout technology (Cui et al., 2011; Geurts et al., 2009; Mashimo et al., 2010).

Here, we report the generation and characterization of single-knockout *Prkdc* (SCID) and double-knockout *Prkdc* and *Il2rg* (F344-*scid gamma* [FSG]) rats.

RESULTS

Generation of SCID Rats Using ZFNs

The design and validation of ZFN reagents targeting the first exon of rat *Prkdc* gene were described previously (Mashimo et al., 2010) (Figure 1A; Figure S1). The validated ZFN mRNA was microinjected into fertilized F344/Stm or Crlj:WI oocytes, which were then transferred into the oviducts of pseudopregnant Crlj:WI female rats (Figure 1B). Screening of 39 newborn animals revealed that 26 of them (66.7%) carried mutations, comprising deletions from 1 bp to 919 bp and a 1-bp insertion (Figures 1C and 1D; Figure S2). The rate and variation of the ZFN-induced mutations were similar to those reported in previous studies (Cui et al., 2011; Geurts et al., 2009; Mashimo et al., 2010). The majority of these were frame-shift mutations resulting in the complete loss of mRNA expression as confirmed by reverse transcriptase (RT)-PCR (Figure 1E) and protein expression as confirmed by western blotting (Figure 1F). Furthermore, double injection of *Prkdc* and

interleukin 2 receptor-gamma (*Il2rg*) ZFN-encoding mRNA into 219 fertilized F344/Stm oocytes resulted in one male carrying 7- and 46-bp deletions in *Prkdc,* and one female carrying 227- and 716-bp deletions in *Prkdc* and a 3-bp deletion in *Il2rg* (Figure 1B).

To clarify whether the ZFNs only induced mutations in the targeted region, we checked 12 sites that showed a high rate of similarity to the targeted site at the sequence level with no more than 7–8 bp mismatches, as illustrated in Table S1. Insertions or deletions were not observed at any of these off-target sites among the ZFN-modified founders. Although we cannot exclude the possibility that the ZFNs cleaved unknown off-target sites, we subsequently excluded such undesired mutations excluded from the genome of the carrier animals by backcrossing to the parental strain. After crossing with wild-type (WT) animals, the ZFN-induced *Prkdc* and *Il2rg* mutations were faithfully transmitted through the germline. Some of the ZFN-modified founders were subsequently bred to homozygosity for use in further experiments.

Growth Retardation in SCID Rats

Heterozygous $Prkdc^{+/-}$ rats were indistinguishable from their WT littermates in all respects. Approximately 25% of the offspring born to $Prkdc^{+/-}$ × $Prkdc^{+/-}$ crosses were homozygous $Prkdc^{-/-}$ rats, and were significantly smaller than their WT and heterozygous littermates (Figure 2A). When the embryos from $Prkdc^{+/-}$ × $Prkdc^{+/-}$ crosses were examined and weighed, a difference in size was observed at embryonic day 14.5 (E14.5), which became statistically significant at E17.5 (Figure 2B). During the 6 month observation period, the $Prkdc^{-/-}$ rats grew and maintained a body weight that was 70% of that of the controls (Figure 2C). $Prkdc^{-/-}$ SCID rats normally survive for at least 1 year under specific pathogen-free conditions. Both male and female $Prkdc^{-/-}$ rats were fertile, but the average litter size was small (4.7 ± 2.0 [n = 9] versus 9.1 ± 1.6 of F344 rats [n = 12]). Newly generated F344-$Prkdc^{-/-}$ $Il2rg^{-/-}$ rats (FSG rats) showed phenotypes similar to those of SCID rats for growth, survival, and reproducibility (Figure 2C).

To further characterize the growth deficiency, we derived primary fibroblasts from WT (+/+), heterozygous (+/−), and homozygous (−/−) rat embryos (rat embryonic fibroblasts [REFs]), and monitored their growth in vitro (Figure 2D). Early-passage $Prkdc^{-/-}$ REFs grew slowly, at a rate 70% of that shown by the $Prkdc^{+/-}$ and $Prkdc^{+/+}$ REFs. This difference was partly due to a decrease in the number of dividing cells within the $Prkdc^{-/-}$ cultures, as determined by incorporating bromodeoxyuridine (BrdU) into chromosomal DNA during an 18 hr labeling period (Figure 2E). Proliferation decreased with passage number, and by passage 4, $Prkdc^{-/-}$ REF cultures contained nondividing giant cells, suggesting premature senescence (Figure 2F). Senescence-associated β-galactosidase (SA-β-Gal) activity assays showed significantly higher numbers of SA-β-Gal-positive cells within $Prkdc^{-/-}$ REF cultures compared with $Prkdc^{+/-}$ or $Prkdc^{+/+}$ REF cultures (Figure 2G). To the best of our knowledge, neither growth retardation nor premature senescence has been reported in SCID mice (Bosma et al., 1983; Gao et al., 1998; Jhappan et al., 1997; Taccioli et al., 1998).

IR Sensitivity and DSB-Repair Defects in SCID REFs

Mouse embryonic fibroblasts (MEFs) from SCID mice or *Prkdc*-deficient mice, and the *Prkdc*-deficient human glioma cell line M059J are all IR-sensitive, although the level of sensitivity varies. When we used a colony survival assay to test IR sensitivity in REF cells, $Prkdc^{-/-}$ REFs were significantly more sensitive than $Prkdc^{+/-}$ or $Prkdc^{+/+}$ REFs (Figure 2H). Accordingly, $Prkdc^{-/-}$ REF cells accumulated foci comprising histone H2AX (γH2AX), a surrogate marker for DSBs, after an exposure to 1 Gy of irradiation (Figure 2I).

We next used a pEJ assay (Kobayashi et al., 2010) and a DR-GFP (Pierce and Jasin, 2005) assay to further examine the effects of *Prkdc*-deficiency on the NHEJ and homologous recombination (HR) pathways, respectively. After the generation of DSBs using I-SecI, the number of GFP-positive $Prkdc^{-/-}$ REFs in the pEJ assay significantly decreased compared with that of $Prkdc^{+/+}$ REFs (Figure 2J), clearly indicating a severe deficiency in the NHEJ pathway in these cells. In contrast, the HR pathway was significantly increased in $Prkdc^{-/-}$ REFs (Figure 2K), suggesting that a deficiency in the NHEJ pathway induces a more active HR pathway as a compensatory mechanism.

Impaired Lymphoid Development in SCID Rats

Gross and microscopic analyses of SCID and FSG rats revealed abnormal lymphoid development (Figures 3A–3D). The thymuses from SCID and FSG rats were extremely hypoplastic (Figure 3A) and comprised an epithelial rudiment without any lymphocytes (Figure 3C). The spleens were also smaller (Figure 3B), with severely hypoplastic white pulp, and red pulp containing myeloid cells (Figure 3D). Serum immunoglobulin (Ig) levels (IgA and IgM) were undetectable in 5-week-old $Prkdc^{-/-}$ rats, whereas IgG levels in $Prkdc^{-/-}$ rats nursed by $Prkdc^{+/-}$ heterozygous mothers were detected at half the levels seen in control $Prkdc^{+/+}$ rats (Figures 3E–3G), confirming the postnatal transfer of maternal IgG previously described in rodents (Gustafsson et al., 1994). IgG levels were lowest in 8-week-old $Prkdc^{-/-}$ rats, and undetectable in 5-week-old $Prkdc^{-/-}$ rats nursed by $Prkdc^{-/-}$ homozygous mothers (Figure 3E). Approximately 20% of young adult (or of the majority of old SCID) mice known to have a "leaky" phenotype showed detectable Ig levels, generated by a few clones of functional B cells (Bosma et al., 1983). To date, none of the SCID rats examined (n = 9, until 1 year of age) have shown a leaky phenotype for serum Ig (Figures 3E–3G).

Consistent with the histology, the number of thymocytes and splenocytes was markedly reduced in SCID and FSG rats compared with control F344 rats (Table S2). In the peripheral blood (PB) profile, the number of white blood cells (WBCs) was reduced in SCID and FSG rats compared with F344 rats (Table S3). Differential counts of WBCs showed a dramatic decrease in leucocytes and relative increases in neutrophils and monocytes in SCID and FSG rats (Table S4).

To further characterize the immunological deficiency in SCID rats, we examined cell populations isolated from the thymus, spleen, and bone marrow (BM) using flow cytometry (Figures 3H–3J). $CD4^+$ or $CD8^+$ single-positive (SP), and $CD4^+CD8^+$ double-positive (DP) T cells were completely absent from SCID

Cell PRESS
Open ACCESS

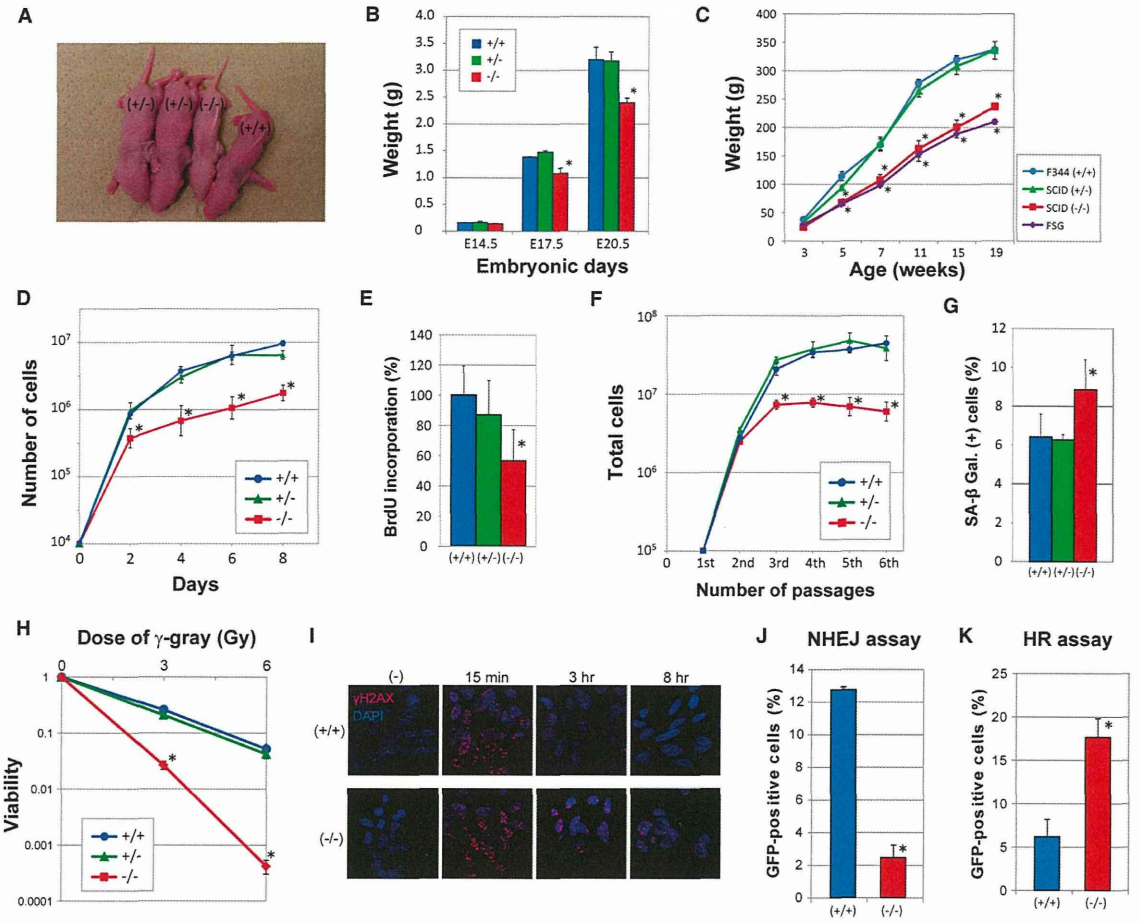

Figure 2. *Prkdc* Deficiency in Rats Results in Growth Retardation, Premature Senescence, and Radiation Sensitivity

(A) Photograph of newborn for *Prkdc*$^{-/-}$, *Prkdc*$^{+/-}$, and WT *Prkdc*$^{+/+}$ littermates.

(B) Development of *Prkdc* (+/+, n = 3; +/−, n = 6; −/−, n = 3) embryos, as measured by weight at E14.5, E17.5, and E20.5.

(C) Postnatal growth of *Prkdc* (+/+, n = 4; +/−, n = 8; −/−, n = 4) and *Prkdc*$^{-/-}$ *Il2rg*$^{-/-}$ FSG (n = 5) rats.

(D) Proliferation of primary fibroblasts from *Prkdc* (+/+, n = 3; +/−, n = 3; −/−, n = 3) E14.5 rats. Second-passage REFs were plated in 60 mm dishes and counted every 2 days.

(E) Division of REFs from *Prkdc* (+/+, n = 3; +/−, n = 3; −/−, n = 3) rats. Incorporation of BrdU into chromosomal DNA was measured after an 18 hr labeling period.

(F) Proliferation of REFs from *Prkdc* (+/+, n = 3; +/−, n = 3; −/−, n = 3) rats at each passage.

(G) Cell staining for senescence-associated SA-β-galactosidase activity. The percentage of SA-β-galactosidase-positive cells in the REF (+/+, n = 3; +/−, n = 3; −/−, n = 3) cells was calculated from the average from three experiments.

(H) Radiation sensitivity of *Prkdc* (+/+, +/−, −/−) REF cell lines. Cells were irradiated with the indicated dose of γ-rays, and viability was analyzed using colony formation assays.

(I) γ-H2AX focus formation assay in *Prkdc* (+/+, −/−) REF cell lines after exposure to 1 Gy of γ-rays. Cells were stained with anti-γ-H2AX antibody as a marker for DSBs.

(J and K) NHEJ activity and HR activity of *Prkdc* (+/+, −/−) REF cell lines. I-SceI expression plasmids were introduced into each REF cell line by electroporation. After 2 days, GFP-positive cells induced through the NHEJ pathway (J) or the HR pathway (K) were analyzed by flow cytometry.

Error bars indicate the mean ± SEM; *p < 0.05 for each genotype by one-way analysis of variance (C–H) or Student's t test (J and K). See also Figure S2.

thymuses but were abundant in control thymuses (Figure 3H). This was clearly different from SCID mice, in which DP T cells are present in the thymus (Gao et al., 1998; Taccioli et al., 1998). CD3^{-}CD45RA^{+} B cells were completely absent from SCID spleens and BM, whereas CD3^{-}CD161a^{+} natural killer (NK) cells were present or even increased (Figures 3I and 3J). NK cell numbers were mostly depleted in the BM and spleens of 5-week-old FSG rats (Figures 3I and 3J).

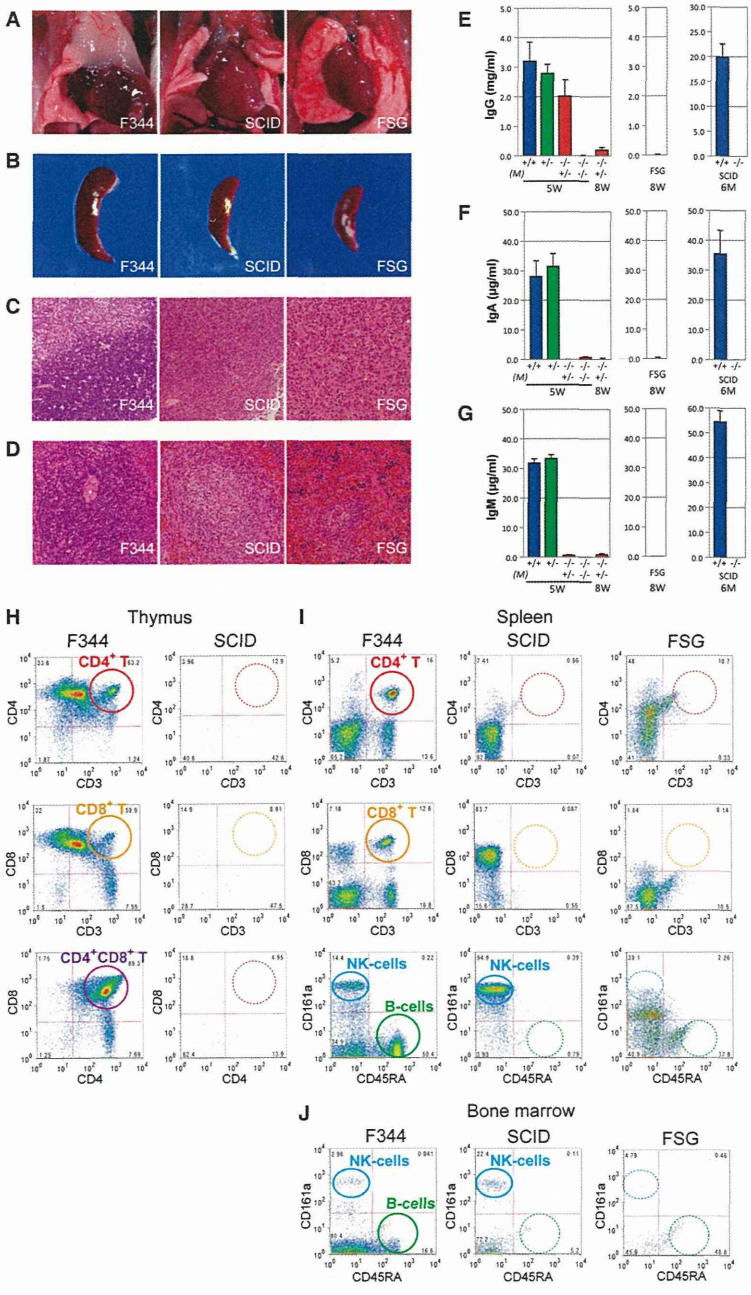

Figure 3. Abnormal Lymphoid Development in *Prkdc*-Deficient SCID Rats

(A and B) Pictures of thymus (A) and spleen (B) from F344, SCID, and FSG rats.

(C) Histological analysis of the thymus (×40). The thymuses of SCID and FSG rats were severely hypoplastic and consisted of an epithelial cell sheet.

(D) Histological analysis of the spleen (×100). In the spleens of SCID and FSG rats, the white pulp was virtually devoid of lymphocytes and the red pulp was occupied by a variety of myeloid cells.

(E–G) ELISA for serum IgG (E), IgA (F), and IgM (G) levels in *Prkdc* SCID (+/+, n = 3; +/−, n = 6; −/−, n = 4) rats. Error bars indicate the mean ± SEM. IgG, IgA, and IgM levels were very low or undetectable in 5-week-old *Prkdc*$^{-/-}$ rats nursed by *Prkdc*$^{-/-}$ homozygous mothers (M: −/−, n = 3), whereas IgG was detected in 5-week-old *Prkdc*$^{-/-}$ rats nursed by a *Prkdc*$^{+/-}$ heterozygous mother (M: +/−, n = 4) at half the levels seen in the control rats, probably due to transfer through the maternal milk. IgG, IgA, and IgM levels were undetectable in 8-week-old FSG rats (n = 4) and 6-month-old *Prkdc*$^{-/-}$ rats (+/+, n = 6; −/−, n = 5).

(H–J) Flow cytometric analysis of cell populations isolated from thymus (H), spleen (I), and BM (J) in SCID and FSG rats. Dot plots represent CD3, CD4, and CD8 cells for demarcation of T cell subpopulations, and CD3, CD45RA, and CD161a cells for differentiation of T cell, B cell, and NK cell subpopulations. CD4^{+} and CD8^{+} SP, and CD4^{+}CD8^{+} DP T cells were absent from SCID thymuses (H). CD3^{-}CD45RA^{+} B cells were absent from the spleens (I) and BM (J) of SCID and FSG rats. CD3^{-}CD161a^{+} NK cells were present in the SCID, but were mostly diminished in FSG rats (I and J).

Xenotransplantation of Human Induced Pluripotent Stem Cells and Tumor Cells

SCID mice can accept transplanted tissues from other species, including humans. We used SCID rats in a teratoma formation assay. Teratomas were induced by inoculation of human induced pluripotent stem (iPS) cells beneath the testis capsule (Takahashi et al., 2007). All SCID (n = 4/4) and FSG (n = 3/3) rats developed tumors, and in most cases, both testes were affected (Figure 4A). Histological examination showed that the lesion had displaced the normal testis and contained solid areas of teratoma. All teratomas contained differentiated tissues representing all three germ layers, including columnar epithelium, pseudostratified ciliated epithelium (endoderm), neural rosettes (ectoderm), cartilage, and adipose tissue (mesoderm; Figures 4B–4F).

To further evaluate the immunological defects, we used SCID and FSG rats as hosts for the xenotransplantation of human ovarian cancer cells (Mashimo et al., 2010). All SCID rats (n = 6/6) developed tumors within 14 days after injection of ovarian cancer cells, whereas control F344 rats showed no evidence of tumor growth

Cell PRESS
Open ACCESS

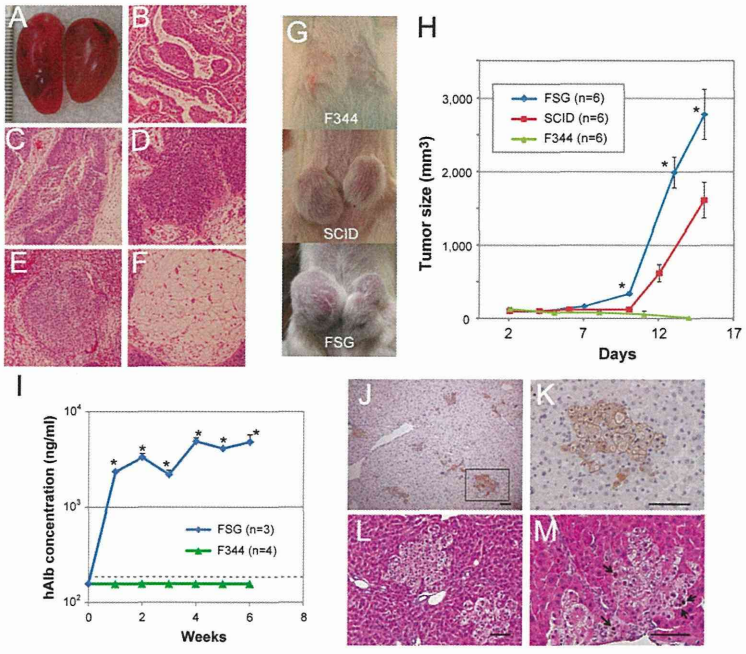

Figure 4. Xenotransplantation of Human iPS Cells, Tumor Cells, and Hepatocytes into SCID and FSG Rats

(A) Teratoma formation assay for human 201B7 iPS cells in the testis of SCID and FSG rats.

(B–F) Histology of differentiated elements found in teratomas: (B) columnar epithelium (endoderm), (C) pseudostratified ciliated epithelium, (D) neural rosettes (ectoderm), (E) cartilage (mesoderm), and (F) adipose tissue.

(G) Subcutaneous injection of human A2780 ovarian cancer cells into F344 (n = 6), SCID (n = 6), and FSG (n = 6) rats.

(H) Growth curve of human ovarian cancer cells. SCID rats developed tumors within 14 days after injection, whereas FSG rats showed more rapid cell proliferation, probably due to the lack of NK cells.

(I–M) Human hepatocytes were transplanted into retrorsine-treated infant FSG (n = 4) and control F344 (n = 3) rats. hAlb was detected in the blood of all transplanted FSG rats (I). The detection limit for hAlb (156.3 ng/ml) is indicated by the dotted line. Error bars indicate the mean ± SEM (H and J). *$p < 0.05$ for SCID versus FSG (H) and for F344 versus FSG (I) by Student's t test.

(J and K) Liver sections stained with human cytokeratin 8/18 (hCK8/18) show engraftment and repopulation of donor human hepatocytes in the recipient rat livers. The sections were counterstained with hematoxylin. The region enclosed by the square in (J) is magnified in (K).

(L) Colonies of cells with a clear cytoplasm were observed in liver sections stained with H&E. The cells were uniform in size, and most were mononuclear.

(M) Proliferated human hepatocytes were labeled with BrdU as shown by arrows. The sections were counterstained with H&E.

Bars = 100 μm (J–M). See also Figure S3.

(n = 0/6; Figure 4G). Of interest, human cancer cells proliferated more rapidly in FSG rats (n = 6/6), presumably due to the lack of NK cell activity in these animals (Figure 4H). The tumors were confirmed by histological analysis, and by PCR using primers to amplify the human MHC class II DQB2 region. These observations illustrate the impaired immune system of SCID and FSG rats, and clearly show that these animals will be useful models for cancer and stem cell research.

Transplantation of Human Hepatocytes and hHSCs

The different metabolic enzyme profiles in human and rat livers are a major limitation for toxicology and drug testing. We generated liver-humanized rats by injecting human hepatocytes into the livers of infant FSG rats pretreated with a pyrrolizidine alkaloid (retrorsine) that is toxic to hepatocytes (Figures 4I–4M). In this study we used FSG rats because they have more immunocompromised states compared with SCID rats, as observed in the tumor cell engraftment. Human albumin (hAlb) was detectable in the blood of all FSG rats (>1 × 10^3 ng/ml, n = 3) 1 week after transplantation (Figure 4I). The hAlb levels increased until 6 weeks after transplantation. However, hAlb was not detectable in F344 control rats (n = 4). Small clusters of human cytokeratin 8/18 (hCK8/18)-positive cells were observed in the livers of the transplanted FSG rats, indicating the successful engraftment and repopulation of human hepatocytes at the tissue level (Figures 4J and 4K). The human hepatocytes within these colonies were morphologically normal but their cytoplasm appeared to be clear (Figure 4L), probably because of the high glycogen content previously reported in liver-humanized mice (Tateno et al., 2004). The BrdU-positive donor cells within the colonies represented the proliferation of engrafted human hepatocytes in the livers of FSG rats (Figure 4M).

The engraftment of hHSCs in immunodeficient mice, such as SCID-hu models (Brehm et al., 2010; Denton and García, 2011; McCune et al., 1989; Pearson et al., 2008; Shultz et al., 2007; Wege et al., 2008), provides an opportunity to study the human immune system in vivo. To test the capability of this feature, we injected human cord blood (hCB) $CD34^+$ cells into 4-week-old FSG rats. During the 3-month monitoring period after transplantation, no human $CD45^+$ cells could be detected in the PB of hHSC-transplanted FSG rats (Figure S3A). Neither human CD3+ T cells nor CD19+ B cells were detected in the PB, spleen, or BM (Figure S3B). Furthermore, 6 months after transplantation, no human $CD45^+$ cells were detected in FSG rats (Figure S3C).

DISCUSSION

In this study, we successfully generated *Prkdc*-deficient SCID rats by using the ZFN technology. The SCID rats were significantly different from SCID mice, in that they showed growth retardation, defects in fibroblast proliferation, and a more severe immunodeficient phenotype. This suggests that DNA-PKcs have

distinct functions in mice and rats. Although few studies have examined spontaneous null mutations in human DNA-PKcs, it has been reported that gene-targeting disruption of human somatic cells results in profound growth retardation, IR sensitivity, and increased genetic instability (Ruis et al., 2008). The most reasonable explanation for the phenotypic differences between mice and humans is that human cells express 50 times more DNA-PK activity than rodent cells (Finnie et al., 1995). Our expression analysis of spleen and fibroblast cells showed that humans express many more DNA-PKcs compared with rodents, and rats express three times more compared with mice (Figure S2). Although DNA-PKcs play a major role in DSB repair (as do other members of the phosphatidylinositol 3-kinase-related kinase [PIKK] family, including ATM and ATR), their exact role is still not completely understood. There are at least three DSB repair pathways: NHEJ, HR, and the alternative NHEJ pathway (Mahaney et al., 2009; Shrivastav et al., 2008; Zha et al., 2011). The pathway used for DSB repair seems to differ between species. NHEJ, in which DNA-PKcs play a key role, is considered to be an error-prone pathway, whereas HR (the major process in lower eukaryotes that lack a DNA-PKcs enzyme) is error-free. Considering that much of the genome in higher eukaryotes comprises less-well-conserved noncoding DNA, NHEJ may have evolved along with DNA-PK activity, particularly in higher mammalian species.

Although SCID mice are the most commonly used experimental animal model for xenograft transplantation, the normal NK cell activity observed in these animals contributes to the limited longevity and function of transplanted human cells (Shultz et al., 2007). Therefore, we additionally generated FSG rats, which show no such NK cell activity. Although both SCID and FSG rats could serve as hosts for xenogeneic cell grafts such as human iPS cells and ovarian cancer cells, the FSG rats showed higher proliferation of human tumor cells than the SCID rats (Figure 4H), indicating a more severely immunocompromised state similar to that reported in *Prkdc*- and *Il2rg*-deficient mice used for xenotransplantation of human melanoma cells (Quintana et al., 2008) or human blood cells (Ishikawa et al., 2005). Further transplantation studies using diverse human cancer cells, such as preclinical cancer cells or cancer stem cells, will be interesting and will improve our understanding of severely immunocompromised hosts.

In addition, we engrafted human hepatocytes into the livers of retrorsine-treated FSG rats (Figure 4I–4M). hAlb was secreted in the blood of transplanted FSG rats, and clusters of human transplanted hepatocytes were observed in the livers of the FSG rats. Liver-humanized rats have several advantages over mouse models: (1) rats are 10 times larger than mice, providing greater blood volumes and more bile acid, cells, and tissues; (2) pharmacological and toxicological data have been accumulated for rats; and (3) it is easier to perform complex surgical experiments in rats. Liver-humanized rats may also allow large-scale and high-quality proliferation of either WT human hepatocytes or iPS-derived hepatocytes, which is currently a considerable obstacle to the culture of human hepatocytes. Liver-humanized rats would provide a robust platform for in vivo toxicological assays and drug metabolism assays. Although the replacement rate of human hepatocytes in the FSG rats was still lower compared than that previously obtained in liver-humanized mice (Azuma et al., 2007; Strom et al., 2010; Tateno et al., 2004) that were genetically modified using either uroplasminogen activator (*uPA*) transgenes (Tateno et al., 2004) or Fumaryl acetoacetate hydrolase (*Fah*) knockouts (Strom et al., 2010), similar genetic alterations in rats will probably also improve the engraftment success in liver-humanized rats.

Despite these successful results for transplantation of human iPS cells, tumor cells, and hepatocytes, the FSG rats rejected transplanted hHSCs (Figure S3). In mice, xenotransplantation in the nonobese diabetic *Prkdc*^{scid} (NOD.SCID) or NOD.*Prkdc*^{scid}.*Il2rg*$^{-/-}$ (NSG or NOG) mouse has become the gold-standard assay for hHSCs, highlighting the importance of the genetic background for such transplantation experiments. Recently, it was shown that the signal regulatory protein alpha (*Sirpa*) of the NOD allele enhances binding to the human CD47 and could provide inhibitory regulation of mouse phagocytes by CD47-SIRPa interaction (the so-called "don't eat me" signal), allowing significantly increased engraftment and maintenance of hHSCs in the mouse BM (Takenaka et al., 2007). This was also supported by experiments in which transgenic mice with human SIRPa in the non-NOD background showed significantly higher levels of human cell engraftment comparable to those in NSG mice (Strowig et al., 2011). Transgenic FSG rats with human SIRPa or NOD-SIRPa may change the BM microenvironment of FSG rats in a way that allows them to accept the engraftment of hHSCs. In addition to *Sirpa*, structural species-specific differences in the BM environment between mice and rats, and differences in the protocols used for HSC engraftment may explain why transplantation of hHSCs fails in FSG rats.

In conclusion, the newly developed SCID and FSG rats described in this study can be a valuable resource in various fields, such as stem cell research and translational research, and serve as an important experimental model for preclinical drug testing. These humanized models will also allow preclinical evaluation of stem-cell-based therapies and expand the options for translational research. This is particularly important in the field of regenerative medicine, because humanized rats can be used to evaluate not only the ability of the cells to engraft but also their therapeutic efficiency. However, additional genetic modifications may be required to permit transplantation of human cells or tissues, such as human hepatocytes and hHSCs.

EXPERIMENTAL PROCEDURES

Generation of Knockout Rats Using ZFNs

Custom-designed ZFN plasmids for the rat *Prkdc* gene and the *Il2rg* gene were obtained from Sigma-Aldrich (St. Louis, MO). The design, cloning, and validation of the ZFNs were performed as previously described (Mashimo et al., 2010). In brief, ZFNs were designed to recognize a site-specific sequence within the first exon of the rat *Prkdc* gene (Figure S4). Approximately 2–3 pl of ZFN mRNA (10 ng/μl) were injected into the pronuclei of embryos collected from F344/Stm or Crlj:WI females as previously described (Mashimo et al., 2010). The cultured embryos were then transferred to the oviducts of pseudo-pregnant females (Crlj:WI, 8–10 weeks). To edit the ZFN cleavage site in the genome at the *Prkdc* locus, two primer sets were designed to amplify small (309 bp) and large (1,321 bp) fragments as shown in Figure S4. The PCR products were directly sequenced using the BigDye terminator v3.1 cycle sequencing mix and the standard protocol for an Applied Biosystems 3130 DNA Sequencer (Carlsbad, CA).

Cell PRESS
Open ACCESS

All animal care and experiments conformed to the Guidelines for Animal Experiments of Kyoto University, and were approved by the Animal Research Committee of Kyoto University. Transplantation studies using human hepatocytes were approved by the Ethics Board of PhoenixBio Co., Ltd. (Higashihiroshima, Japan). All SCID rats were maintained under specific pathogen-free conditions. The SCID rats are deposited in the National BioResource Project–Rat in Japan (http://www.anim.med.kyoto-u.ac.jp/nbr).

RT-PCR and Western Blotting

Total RNA was extracted from the spleens of 5-week-old rats using Isogen reagent (Nippon Gene, Tokyo, Japan). RT-PCR was performed using the primers for *Prkdc* described in Figure S2, and with *Gapdh* 5′-GGCACAGT CAAGGCTGAGAATG-3′ and 5′-ATGGTGGTGAAGACGCCAGTA-3′. Western blotting was carried out using cell lysates from the spleens of 5-week-old rats according to standard methods. Signals were detected with antibodies against rat PRKDC (H-163; Santa Cruz Biotechnology, Santa Cruz, CA) and β-actin (AC-40; Sigma Aldrich).

REF Culture, Proliferation Assays, and SA-β-Galactosidase Assay

REFs were isolated from embryos after 14.5 days of gestation from the female partners of intercrossed *Prkdc*$^{+/-}$ rats. To obtain a growth curve, passage 2 REFs (2×10^4) were plated on six-well plates in triplicate. The cells were trypsinized, stained with trypan blue, and counted every other day for a total of 8 days. For the BrdU incorporation assay, cells were plated with BrdU (100 μM) and labeled for 48 hr in 96-well plates. The cells were stained with the anti-BrdU-POD antibody and quantified by measuring the absorbance with an enzyme-linked immunosorbent assay (ELISA) reader (BrdU Labeling and Detection Kit III; Roche Applied Science, Indianapolis, IN). To assess SA-β-galactosidase activity, cells were plated 60 mm dishes and stained for 24 hr. The percentage of SA-β-galactosidase-positive cells was determined by manually counting the number of blue cells (Senescence Detection Kit; BioVision, Mountain View, CA) within the total cell population.

Preparation of Immortalized REF Cells

Generation of immortalized REF cells by human telomerase reverse transcriptase (hTERT) was performed as previously described (Nakamura et al., 2002). Briefly, rat primary fibroblasts (+/+, +/−, or −/−) were infected with an hTERT-introduced retrovirus and then continuously cultured with G418. After a few weeks, viable cells were infected with SV40 and then continuously cultured for >1 month. These transformed cells (REF-hTERT/SV) were used for radiation sensitivity assays, and HR and NHEJ assays.

Radiation Sensitivity Assay and Immunofluorescence Staining for γ-H2AX Foci

For the radiation sensitivity assays, the cells were trypsinized and irradiated with 3 or 5 Gy of ^{60}Co γ-rays at a dose rate of 1.1 Gy/min. Immediately after irradiation, the cells were plated into 100 mm dishes at a density such that 50–200 cells would survive, and then incubated for 10 days. The dishes were then fixed with ethanol and stained with 3% Giemsa, and the number of colonies was counted. The surviving fractions were calculated by comparing the number of colonies formed by irradiated cells with the number of colonies formed by nonirradiated control cells. Each result represents an average value from three independent experiments.

Immunostaining for γ-H2AX foci was performed as previously described (Kobayashi et al., 2010). Cells grown on a glass slide were fixed with cold methanol for 15 min, rinsed with cold acetone several times, and then air-dried. Anti-γ-H2AX antibody (Upstate: #05-636) and Alexa-596-conjugated anti-mouse IgG antibodies (Molecular Probes, Carlsbad, CA) were to visualize the γ-H2AX foci.

NHEJ and HR Assays

NHEJ and HR assays were performed as previously described (Kobayashi et al., 2010; Pierce and Jasin, 2005). The cells were generated from REF-hTERT/SV cells via introduction of a pEJ construct for the NHEJ assay or a DR-GFP construct for the HR assay. To measure the repair of I-SceI-generated DSBs, 50 μg of the I-SceI expression vector (pCBASce) was introduced into 1×10^6 cells by electroporation (GenePulser; Bio-Rad, Hercules, CA). To determine the level of NHEJ or HR repair, the percentage of GFP-positive cells was quantified by flow cytometry (FACSCalibur; Becton Dickinson, Franklin Lakes, NJ) 3 days after electroporation.

Immunofluorescence and Fluorescence-Activated Cell-Sorting Analysis

PB specimens were collected from the caudal vena cava. Serum Ig levels were measured by ELISA using Rat IgG, IgA, and IgM ELISA quantitation kits (Bethyl Laboratories, Montgomery, TX). For histopathology, tissues were fixed in Bouin's fluid and embedded in paraffin. The embedded tissues were then sectioned (5–7 μm thick) at room temperature and stained with hematoxylin and eosin (H&E) to permit evaluation by light microscopy.

Flow cytometric analysis of cell populations isolated from thymus, BM, and spleen were carried out using IOTest Anti-Rat CD3-FITC/CD45RA-PC7/CD161a-APC (Beckman Coulter, Fullerton, CA) to differentiate the T cell, B cell, and NK cell subpopulations, and IOTest Anti-Rat CD3-FITC/CD4-PC7/CD8-APC (Beckman Coulter) to enumerate the T cell subpopulations. Anti-CD45 monoclonal antibodies (Beckman Coulter) were used for the intracellular staining of lymphocytes. Mouse IgM, IgG1, and IgG2a antibodies (Beckman Coulter) were used as isotype-matched controls. The cell samples were treated with FcR-blocking reagent (Miltenyi Biotec, Auburn, CA) for 10 min, stained with the fluorochrome-conjugated antibodies for 30 min, and washed three times with PBS/10% FCS. Stained cell samples were analyzed with the use of a four-color fluorescence-activated cell-sorting (FACS) flow cytometer (FACSCalibur; Becton Dickinson) and the data were analyzed with CellQuest software (Becton Dickinson).

Teratoma Formation by Human iPS Cells

Human iPS cells (201B7) were supplied by the Center for iPS Cell Research and Application, Kyoto University (Kyoto, Japan). Clumps of ~2×10^5 human iPS cells with an undifferentiated morphology were harvested at the time of routine passage as described previously (Takahashi et al., 2007), and injected into the testis of 6- to 8-week-old rats. Six to 8 weeks later, when testicular lesions developed and were palpable, the resulting tumors were dissected, fixed in 10% neutral buffered formalin, embedded in paraffin, and examined histologically after H&E staining.

Tumor Cell Xenotransplantation

The human ovarian cancer cell line A2780 was purchased from the European Collection of Cell Cultures (ECACC, Wiltshire, UK). Cells were cultured in RPMI 1640 medium (GIBCO, Fort Worth, TX) with 10% heat-inactivated FBS (Hyclone, Logan, UT). Subcutaneous injections of 2×10^5 A2780 cells plus Matrigel (Becton Dickinson) were performed on 5-week-old female rats. Tumors were measured (length [*a*] and width [*b*]) in millimeters using calipers, and tumor volumes (*V*) were calculated using the formula $V = ab^2/2$, where *a* is the longer of the two measurements. Human-specific PCR primers were designed to amplify major histocompatibility complex class II DQ beta 2 (HLA-DQB2) at exon 4 as follows: 5′-CCTAGGGTGGTCAGACTGGA-3′ and 5′-AAAATCCCCCAAAACAAAGG-3′.

Transplantation of Human Hepatocytes

Human hepatocytes were isolated from human-hepatocyte chimeric mice (PXB mice, http://www.phoenixbio.co.jp) using the two-step collagenase perfusion method as described previously (Yamasaki et al., 2010). The donor cells (cryopreserved human hepatocytes derived from a 5-year-old boy) were purchased from BD Gentest (Becton Dickinson). Two-week-old rats were given intraperitoneal injections of retrorsine (Sigma-Aldrich) at 10 mg/kg body weight. Seven days after retrorsine treatment, the isolated human hepatocytes (5 or 10×10^5 viable cells) were transplanted into the animals via the portal vein. To deplete Kupffer cells, the rats were injected intraperitoneally with 10 ml/kg of liposome-encapsulated clodronate 2 days before and 3 days after transplantation. Plasma samples were collected weekly and hAlb levels were measured by ELISA (Human Serum Albumin ELISA Quantitation Kit; Bethyl Laboratories). The rat livers were harvested 6 weeks after transplantation. When necessary, BrdU (50 mg/kg; Sigma-Aldrich) was injected intraperitoneally 1 hr before sacrifice. Paraffin and frozen sections (5 μm thick) were prepared from the liver tissues and subjected to H&E or

immunohistochemical staining using human-specific hCK8/18 mouse monoclonal antibodies (NCL5D3; MP Biomedicals, Aurora, OH) or BrdU mouse monoclonal antibodies (Bu20a; Dako Cytomation, Glostrup, Denmark). The antibodies were visualized with a Vectastain ABC Kit (Vector Laboratories, Burlingame, CA) using DAB substrates.

SUPPLEMENTAL INFORMATION

Supplemental Information includes Extended Experimental Procedures, four figures, and five tables and can be found with this article online at http://dx.doi.org/10.1016/j.celrep.2012.08.009.

LICENSING INFORMATION

ACKNOWLEDGMENTS

We thank Jean-Louis Guenet for helpful discussion. This study was supported in part by a Grant-in-Aid for Research on New Drug Development from the Ministry of Health, Labor and Welfare of Japan, and by the Industrial Technology Research Grant Program in 2008, New Energy, and the Industrial Technology Development Organization of Japan.

Received: October 26, 2011
Revised: May 8, 2012
Accepted: August 9, 2012
Published online: September 13, 2012

REFERENCES

Azuma, H., Paulk, N., Ranade, A., Dorrell, C., Al-Dhalimy, M., Ellis, E., Strom, S., Kay, M.A., Finegold, M., and Grompe, M. (2007). Robust expansion of human hepatocytes in Fah-/-/Rag2-/-/Il2rg-/- mice. Nat. Biotechnol. *25*, 903–910.

Baiocchi, M., Biffoni, M., Ricci-Vitiani, L., Pilozzi, E., and De Maria, R. (2010). New models for cancer research: human cancer stem cell xenografts. Curr. Opin. Pharmacol. *10*, 380–384.

Bosma, G.C., Custer, R.P., and Bosma, M.J. (1983). A severe combined immunodeficiency mutation in the mouse. Nature *301*, 527–530.

Brehm, M.A., Shultz, L.D., and Greiner, D.L. (2010). Humanized mouse models to study human diseases. Curr. Opin. Endocrinol. Diabetes Obes. *17*, 120–125.

Cui, X., Ji, D., Fisher, D.A., Wu, Y., Briner, D.M., and Weinstein, E.J. (2011). Targeted integration in rat and mouse embryos with zinc-finger nucleases. Nat. Biotechnol. *29*, 64–67.

Denton, P.W., and García, J.V. (2011). Humanized mouse models of HIV infection. AIDS Rev. *13*, 135–148.

Finnie, N.J., Gottlieb, T.M., Blunt, T., Jeggo, P.A., and Jackson, S.P. (1995). DNA-dependent protein kinase activity is absent in xrs-6 cells: implications for site-specific recombination and DNA double-strand break repair. Proc. Natl. Acad. Sci. USA *92*, 320–324.

Franco, S., Alt, F.W., and Manis, J.P. (2006). Pathways that suppress programmed DNA breaks from progressing to chromosomal breaks and translocations. DNA Repair (Amst.) *5*, 1030–1041.

Gao, Y., Chaudhuri, J., Zhu, C., Davidson, L., Weaver, D.T., and Alt, F.W. (1998). A targeted DNA-PKcs-null mutation reveals DNA-PK-independent functions for KU in V(D)J recombination. Immunity *9*, 367–376.

Geurts, A.M., Cost, G.J., Freyvert, Y., Zeitler, B., Miller, J.C., Choi, V.M., Jenkins, S.S., Wood, A., Cui, X., Meng, X., et al. (2009). Knockout rats via embryo microinjection of zinc-finger nucleases. Science *325*, 433.

Gustafsson, E., Mattsson, A., Holmdahl, R., and Mattsson, R. (1994). Pregnancy in B-cell-deficient mice: postpartum transfer of immunoglobulins prevents neonatal runting and death. Biol. Reprod. *51*, 1173–1180.

Ishikawa, F., Yasukawa, M., Lyons, B., Yoshida, S., Miyamoto, T., Yoshimoto, G., Watanabe, T., Akashi, K., Shultz, L.D., and Harada, M. (2005). Development of functional human blood and immune systems in NOD/SCID/IL2 receptor gamma chain(null) mice. Blood *106*, 1565–1573.

Ito, M., Kobayashi, K., and Nakahata, T. (2008). NOD/Shi-scid IL2rgamma(null) (NOG) mice more appropriate for humanized mouse models. Curr. Top. Microbiol. Immunol. *324*, 53–76.

Izsvák, Z., Fröhlich, J., Grabundzija, I., Shirley, J.R., Powell, H.M., Chapman, K.M., Ivics, Z., and Hamra, F.K. (2010). Generating knockout rats by transposon mutagenesis in spermatogonial stem cells. Nat. Methods *7*, 443–445.

Jhappan, C., Morse, H.C., 3rd, Fleischmann, R.D., Gottesman, M.M., and Merlino, G. (1997). DNA-PKcs: a T-cell tumour suppressor encoded at the mouse scid locus. Nat. Genet. *17*, 483–486.

Katoh, M., Tateno, C., Yoshizato, K., and Yokoi, T. (2008). Chimeric mice with humanized liver. Toxicology *246*, 9–17.

Kneteman, N.M., and Mercer, D.F. (2005). Mice with chimeric human livers: who says supermodels have to be tall? Hepatology *41*, 703–706.

Kobayashi, J., Kato, A., Ota, Y., Ohba, R., and Komatsu, K. (2010). Bisbenzamidine derivative, pentamidine represses DNA damage response through inhibition of histone H2A acetylation. Mol. Cancer *9*, 34.

Leonard, W.J. (2001). Cytokines and immunodeficiency diseases. Nat. Rev. Immunol. *1*, 200–208.

Mahaney, B.L., Meek, K., and Lees-Miller, S.P. (2009). Repair of ionizing radiation-induced DNA double-strand breaks by non-homologous end-joining. Biochem. J. *417*, 639–650.

Mashimo, T., Yanagihara, K., Tokuda, S., Voigt, B., Takizawa, A., Nakajima, R., Kato, M., Hirabayashi, M., Kuramoto, T., and Serikawa, T. (2008). An ENU-induced mutant archive for gene targeting in rats. Nat. Genet. *40*, 514–515.

Mashimo, T., Takizawa, A., Voigt, B., Yoshimi, K., Hiai, H., Kuramoto, T., and Serikawa, T. (2010). Generation of knockout rats with X-linked severe combined immunodeficiency (X-SCID) using zinc-finger nucleases. PLoS ONE *5*, e8870.

McCune, J.M., Kaneshima, H., Lieberman, M., Weissman, I.L., and Namikawa, R. (1989). The scid-hu mouse: current status and potential applications. Curr. Top. Microbiol. Immunol. *152*, 183–193.

Meuleman, P., Libbrecht, L., De Vos, R., de Hemptinne, B., Gevaert, K., Vandekerckhove, J., Roskams, T., and Leroux-Roels, G. (2005). Morphological and biochemical characterization of a human liver in a uPA-SCID mouse chimera. Hepatology *41*, 847–856.

Nakamura, H., Fukami, H., Hayashi, Y., Kiyono, T., Nakatsugawa, S., Hamaguchi, M., and Ishizaki, K. (2002). Establishment of immortal normal and ataxia telangiectasia fibroblast cell lines by introduction of the hTERT gene. J. Radiat. Res. (Tokyo) *43*, 167–174.

O'Driscoll, M., and Jeggo, P.A. (2006). The role of double-strand break repair - insights from human genetics. Nat. Rev. Genet. *7*, 45–54.

Pearson, T., Greiner, D.L., and Shultz, L.D. (2008). Humanized SCID mouse models for biomedical research. Curr. Top. Microbiol. Immunol. *324*, 25–51.

Perryman, L.E. (2004). Molecular pathology of severe combined immunodeficiency in mice, horses, and dogs. Vet. Pathol. *41*, 95–100.

Pierce, A.J., and Jasin, M. (2005). Measuring recombination proficiency in mouse embryonic stem cells. Methods Mol. Biol. *291*, 373–384.

Quintana, E., Shackleton, M., Sabel, M.S., Fullen, D.R., Johnson, T.M., and Morrison, S.J. (2008). Efficient tumour formation by single human melanoma cells. Nature *456*, 593–598.

Ruis, B.L., Fattah, K.R., and Hendrickson, E.A. (2008). The catalytic subunit of DNA-dependent protein kinase regulates proliferation, telomere length, and genomic stability in human somatic cells. Mol. Cell. Biol. *28*, 6182–6195.

Shrivastav, M., De Haro, L.P., and Nickoloff, J.A. (2008). Regulation of DNA double-strand break repair pathway choice. Cell Res. *18*, 134–147.

Shultz, L.D., Ishikawa, F., and Greiner, D.L. (2007). Humanized mice in translational biomedical research. Nat. Rev. Immunol. *7*, 118–130.

Strom, S.C., Davila, J., and Grompe, M. (2010). Chimeric mice with humanized liver: tools for the study of drug metabolism, excretion, and toxicity. Methods Mol. Biol. *640*, 491–509.

Strowig, T., Rongvaux, A., Rathinam, C., Takizawa, H., Borsotti, C., Philbrick, W., Eynon, E.E., Manz, M.G., and Flavell, R.A. (2011). Transgenic expression of human signal regulatory protein alpha in Rag2-/-gamma(c)-/- mice improves engraftment of human hematopoietic cells in humanized mice. Proc. Natl. Acad. Sci. USA *108*, 13218–13223.

Taccioli, G.E., Amatucci, A.G., Beamish, H.J., Gell, D., Xiang, X.H., Torres Arzayus, M.I., Priestley, A., Jackson, S.P., Marshak Rothstein, A., Jeggo, P.A., and Herrera, V.L. (1998). Targeted disruption of the catalytic subunit of the DNA-PK gene in mice confers severe combined immunodeficiency and radiosensitivity. Immunity *9*, 355–366.

Takahashi, K., Tanabe, K., Ohnuki, M., Narita, M., Ichisaka, T., Tomoda, K., and Yamanaka, S. (2007). Induction of pluripotent stem cells from adult human fibroblasts by defined factors. Cell *131*, 861–872.

Takenaka, K., Prasolava, T.K., Wang, J.C., Mortin-Toth, S.M., Khalouei, S., Gan, O.I., Dick, J.E., and Danska, J.S. (2007). Polymorphism in Sirpa modulates engraftment of human hematopoietic stem cells. Nat. Immunol. *8*, 1313–1323.

Tateno, C., Yoshizane, Y., Saito, N., Kataoka, M., Utoh, R., Yamasaki, C., Tachibana, A., Soeno, Y., Asahina, K., Hino, H., et al. (2004). Near completely humanized liver in mice shows human-type metabolic responses to drugs. Am. J. Pathol. *165*, 901–912.

Tesson, L., Usal, C., Ménoret, S., Leung, E., Niles, B.J., Remy, S., Santiago, Y., Vincent, A.I., Meng, X., Zhang, L., et al. (2011). Knockout rats generated by embryo microinjection of TALENs. Nat. Biotechnol. *29*, 695–696.

Tong, C., Li, P., Wu, N.L., Yan, Y., and Ying, Q.L. (2010). Production of p53 gene knockout rats by homologous recombination in embryonic stem cells. Nature *467*, 211–213.

van der Burg, M., Ijspeert, H., Verkaik, N.S., Turul, T., Wiegant, W.W., Morotomi-Yano, K., Mari, P.O., Tezcan, I., Chen, D.J., Zdzienicka, M.Z., et al. (2009). A DNA-PKcs mutation in a radiosensitive T-B- SCID patient inhibits Artemis activation and nonhomologous end-joining. J. Clin. Invest. *119*, 91–98.

Wege, A.K., Melkus, M.W., Denton, P.W., Estes, J.D., and Garcia, J.V. (2008). Functional and phenotypic characterization of the humanized BLT mouse model. Curr. Top. Microbiol. Immunol. *324*, 149–165.

Yamasaki, C., Kataoka, M., Kato, Y., Kakuni, M., Usuda, S., Ohzone, Y., Matsuda, S., Adachi, Y., Ninomiya, S., Itamoto, T., et al. (2010). In vitro evaluation of cytochrome P450 and glucuronidation activities in hepatocytes isolated from liver-humanized mice. Drug Metab. Pharmacokinet. *25*, 539–550.

Yan, C.T., Boboila, C., Souza, E.K., Franco, S., Hickernell, T.R., Murphy, M., Gumaste, S., Geyer, M., Zarrin, A.A., Manis, J.P., et al. (2007). IgH class switching and translocations use a robust non-classical end-joining pathway. Nature *449*, 478–482.

Zha, S., Jiang, W., Fujiwara, Y., Patel, H., Goff, P.H., Brush, J.W., Dubois, R.L., and Alt, F.W. (2011). Ataxia telangiectasia-mutated protein and DNA-dependent protein kinase have complementary V(D)J recombination functions. Proc. Natl. Acad. Sci. USA *108*, 2028–2033.

実験ガイド

ヒト肝細胞キメラマウスを用いた抗肝炎ウイルス薬効評価系

加国雅和
Masakazu KAKUNI
(株)フェニックスバイオ受託試験部長

立野知世
Chise TATENO
(株)フェニックスバイオ取締役，研究開発部長兼生産部長

1 はじめに

ヒト肝細胞キメラマウス(PXBマウス)は，マウス肝細胞がヒト肝細胞によって置き換えられたマウスであり，2001年に初めて作製例が報告された.[1,2] 従来，ヒト肝細胞を利用して様々な実験が行われてきたが，*in vitro* の実験環境下では単離されたヒト肝細胞の機能が著しく低下・消失するため，得られる実験結果は限定的な内容にならざるを得なかった．しかしヒト肝細胞キメラマウスの肝臓組織内において，ヒト肝細胞は正常に近い立体的組織構造を再構築し，また細胞機能が *in vitro* の実験環境と比較して極めて *in vivo* のヒト肝臓に近いため，PXBマウスは，ヒト肝細胞に関連する様々な研究の進展に大きく貢献している．

本稿では，PXBマウスの主要な用途の1つである，抗肝炎ウイルス薬効評価系について紹介する．なお以下の内容は，筆者らが所属する当社において作製しているPXBマウスに関するものである．

2 肝炎ウイルス感染モデルの概要

ヒト肝細胞キメラマウスの作製には，インフォームドコンセントに基づいてドナーから提供された凍結ヒト肝細胞とホストマウス(uPA/SCIDマウス)を利用する．uPA/SCIDマウスの特徴は，肝障害と重症複合免疫不全の形質を持っていることである．肝障害の形質は，遺伝子導入されたマウスウロキナーゼタイププラスミノーゲンアクチベーター(uPA)が肝細胞に特異的に発現することによってもたらされている．uPAの発現によって，uPA/SCIDマウスの肝細胞は細胞分裂・増殖能が低下している．この形質が，後に導入されるヒト肝細胞の分裂・増殖に都合の良い環境を与えると考えられている．また重症複合免疫不全の形質は，遺伝子の突然変異によって機能的なTおよびBリンパ球が欠損していることによってもたらされている．免疫不全の形質は，マウスにとって異物であるヒト肝細胞を受け入れるために必須の形質である．

ホストマウスへのヒト肝細胞の導入は，生後約3週に実施している．ヒト肝細胞を融解して所定の細胞濃度に調整した後，1匹当たり0.2～1.0×10^6個の細胞を脾臓に注入移植する．脾臓に注入されたヒト肝細胞は，門脈を経由して肝臓に到達した後に肝細胞索内に定着して増殖を開始する．移植後約7週間が経過すると，マウス肝細胞の70%以上がヒト肝細胞によって置換されたPXBマウスが利用可能となる．なお，ヒト肝細胞の置換状況は，マウス血液中に分泌されるヒトアルブミンの濃度を指標としている.[3]

肝炎ウイルス感染モデルの作製例として，C型肝炎ウイルス(HCV)感染PXBマウスモデルおよびB型肝炎ウイルス(HBV)感染PXBマウスモデルの作製方法について紹介する．モデル作製には，PXBマウスのほかに感染源が必要となる．オリジナルの感染源には，肝炎ウイルスに感染した患者の血清や *in vitro* で作製された肝炎ウイルスを含む培養上清を外部機関から入手して利用している．これらのオリジナル感染源をPXBマウスを利用して継代・増幅し，数千匹程度の肝炎ウイルス感染モデル作製に十分な量のマウス血清ストックを確保する．

肝炎ウイルス感染モデル作製には，感染源をおよそ1.0×10^4コピー(ウイルス由来の核酸測定数を単位とする．HCVではRNA，HBVではDNAを測定対象とする)の濃度でPXBマウスの静脈内に接種している．感染源接種後，PXBマウスの血清中でウイルス濃度が定常に到達したことを確認した後に実験を開始する．なお，PXBマウス血清中のウイルス濃度が定常に到達するまでの期間の目安は，

HCVでは約4週間，HBVでは約8週間であるが，これらの期間は，ドナー肝細胞やウイルスの遺伝子型(ジェノタイプ)に依存している．

3 薬効試験例

肝炎ウイルス感染モデルを利用した抗肝炎ウイルス薬効評価試験の具体例を紹介する．3種類の異なるジェノタイプのHCVに感染したPXBマウスを利用して，ペグインターフェロンアルファ2a(Peg-IFNα-2a)による治療効果を検討した試験の結果を図1に示す．PXBマウスの作製に利用したドナーは，BD Bioscience社から購入したBD 85(ドナー詳細；5歳齢，黒人，男児)，感染源にはHCVジェノタイプ1a，1bおよび2aを利用した．感染源接種後，血清中HCV RNA濃度がプラトーに達した5または6週より，Peg-IFNα-2aを30μg/kgの用量で，1週間に2回の頻度で2週間反復皮下投与(投与開始日をday 0としてday 0，3，7，10)した．投与期間終了後には2週間の休薬期間を設けた．試験期間中のday 0，3，7，10の投与前とday 14，17，21，24，28にそれぞれ血液を20μL採取し，得られた血清中のHCV RNA濃度を定量してPeg-IFNα-2aの薬効を確認した．

その結果，Peg-IFNα-2aの投与によってすべてのジェノタイプの血清中HCV RNA濃度が減少した．減少の程度はジェノタイプによって異なり，1aではday 10に5.90%(day 0比)まで，1bではday 10に0.74%まで，2aではday 7～21の期間に0.17%未満(検出下限未満のため)まで減少した．Peg-IFNα-2aの投与終了後は，すべてのジェノタイプにおいて血清中HCV RNA濃度が緩やかに回復し，day 28時点での回復の程度は，1aでは78.95%(day 0比)，1bでは11.71%，2aでは1.09%であった．

次に，HBV感染PXBマウスモデルを利用して，lamivudine(ラミブジン)またはPeg-IFNα-2aによる治療効果を検討した試験の結果を図2に示す．PXBマウスの作製に利用したドナーはBD 85，感染源にはHBVジェノタイプCを利用した．感染源接種後およそ10週より，ラミブジンを30 mg/kgの用量で，1日1回の頻度で2週間反復経口投与した．また，Peg-IFNα-2aは30μg/kgの用量で1週間に2回の頻度で2週間反復皮下投与(投与開始日をday 0としてday 0，3，7，10)した．休薬期間として2週間を設け，対照群には蒸留水を1日1回の頻度で2週間反復経口投与した．試験期間中のday 0，3，7，10の投与前とday 14，17，21，24，28にそれぞれ血液を50μL採取し，得られた血清中のHBV DNA濃度を定量してラミブジンとPeg-IFNα-2aの薬効を確認した．

その結果，ラミブジン投与群およびPeg-IFNα-2a投与群共に，血清中HBV DNA濃度の減少が確

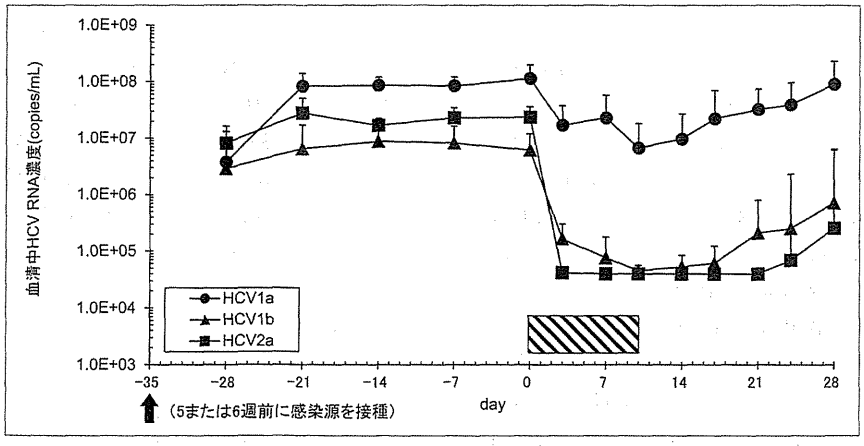

図1 異なるジェノタイプのHCV感染PXBマウスモデルでの治療薬応答性

各値は，平均値＋標準偏差(HCV 1aおよびHCV 2aはn=5，HCV 1bはn=3)を示す．
矢印：感染源接種日，斜線：Peg-IFNα2a投与期間．

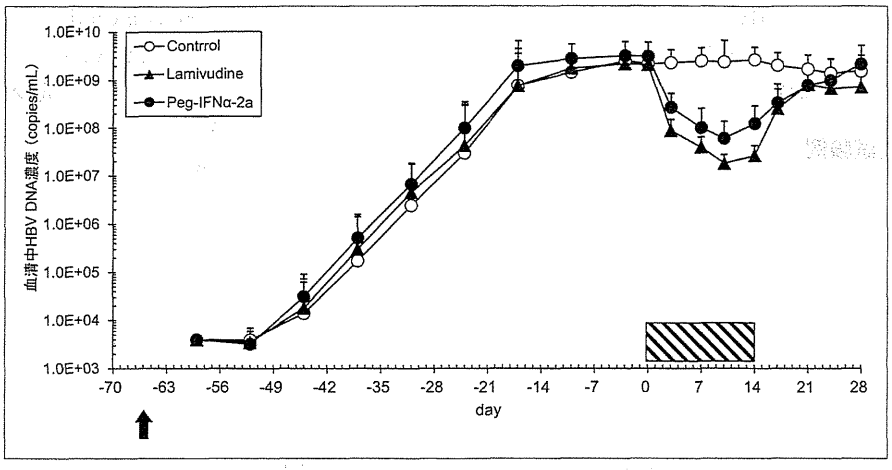

図2　HBV感染PXBマウスモデルでの治療薬応答性

各値は平均値＋標準偏差(n=5)を示す.
矢印：感染源接種日，斜線：薬剤投与期間.

認された．減少の程度は，ラミブジン投与群ではday 10にday 0を基準として1.00%まで低下し，Peg-IFNα-2a投与群ではday 10にday 0を基準として2.08%まで低下した．休薬期間中にはラミブジン投与群およびPeg-IFNα-2a投与群共に血清中HBV DNA濃度が回復し，ラミブジン投与群ではday 28までにday 0を基準として37.64%まで回復した．Peg-IFNα-2a投与群では，day 28までにday 0を基準として73.15%まで回復した．

なお，上記のような抗肝炎ウイルス薬効評価試験から得られる結果を正確に理解するために，肝炎ウイルス感染PXBマウスモデルを利用する際の留意点を以下に示す．まず，評価化合物の作用機序について，このモデルは肝細胞のみがヒト由来であり，かつ，免疫不全の背景を持つために，ヒト肝細胞またはウイルスに直接作用する化合物の評価は可能であるが，免疫系やその他の因子を介して間接的に作用する化合物の評価には適さないと考えられる．次に，臨床での治療効果の予測について，当モデルはヒト肝細胞に患者由来の感染源を感染させているため，臨床での化合物の治療効果を定性的に予測することは可能であるが，ヒト肝細胞以外はマウスであるため，多くの動物モデルと同様に，化合物の用量と治療効果の相関性を定量的に予測するレベルには至っていない．

4　おわりに

肝炎ウイルス感染PXBマウスモデルを利用して，肝炎治療薬の治療効果が確認できることを紹介した．このような肝炎治療薬の検討は，既に肝炎ウイルスに感染した患者の治療を適用対象としたものであるが，ウイルスを感染させる前のPXBマウスを利用することによって，新規感染を防御する効果を検討することも可能である．

これらの評価は，現在，肝炎領域の医薬品候補化合物のスクリーニング／プロファイリングに広く利用されている.[4,5] 肝炎ウイルスの検討では，チンパンジーに代表される類人猿が最も適切なモデル動物として利用されてきたが，倫理的な制約から十分な実験環境が得られない状況が続いていた．PXBマウスの登場は，このような状況を打開し，肝炎治療薬ならびに肝炎感染予防薬の開発に大きく貢献していると考えられる．

参考文献

1) Dandri M. *et al*., *Hepatology*, 33, 981-988 (2001).
2) Mercer D. F. *et al*., *Nat. Med*., 7, 927-933 (2001).
3) Tateno C. *et al*., *Am. J. Pathol*., 165, 901-912 (2004).
4) Kamiya N. *et al*., *J. Gen. Virol*., 91, 1668-1677 (2010).
5) Lupberger J. *et al*., *Nat. Med*., 17, 589-596 (2011).

〔生化学　第84巻　第8号，pp. 699-706，2012〕

特集：肝臓の発生・再生

ヒト肝細胞キメラマウス—肝臓肥大のメカニズムに関して—

立野知世

我々は，ヒト肝細胞を持つキメラマウスを開発した．キメラマウス肝臓は，ヒト肝細胞とマウス非実質細胞で構築されている．キメラマウス肝臓のヒト肝細胞はヒト肝臓におけるヒト肝細胞に近い遺伝子発現，タンパク質発現，活性を示し，組織学的にもほぼ正常な肝臓組織構築を呈している．しかしながら，ヒト肝細胞キメラマウスでは，正常なヒトやマウスとは異なる性質も示す．その一つとして，肝臓の肥大が挙げられる．本稿では，ヒト肝細胞キメラマウスとラット肝細胞キメラマウスでの肝細胞の増殖，遺伝子，タンパク質発現を比較することにより，肝臓肥大のメカニズムに関して考察する．

1. はじめに

肝臓は，成体の肝臓を2/3切除しても残余肝が増殖し，げっ歯類では1週間で元の重量に戻ることから，成体になってもなお高い増殖能力を持つ臓器として知られている．しかしながら，肝細胞をコラゲナーゼ灌流法で分離し*in vitro*で培養すると，その高い増殖能を再現させることは現在のところ不可能である．また，肝細胞を2次元培養することにより，多くの遺伝子やタンパク質の発現が低下する．このことから，特にヒト肝細胞の*in vivo*での増殖・分化に関する性質は不明な点が多い．

Heckelらは生まれながら肝細胞の増殖に障害のあるトランスジェニックマウスを作製した．アルブミンエンハンサー／プロモーター下にウロキナーゼ型プラスミノーゲンアクチベーター（urokinase-type plasminogen activator, uPA）のゲノム遺伝子が約5個連結された形でベクターが導入されているトランスジェニックマウス（Alb-uPAマウス）である[1]．Rhimらは生後5〜11日目のAlb-uPAマウスの脾臓から正常なマウス肝細胞を移植すると，移植したマウス肝細胞が宿主であるAlb-uPAマウスの肝臓に生着・増殖し完全に置換することを示した[2]．彼らはさらにAlb-uPAマウスとヌードマウスを掛け合わせることにより，Alb-uPA/ヌードマウスを作製し，ラット肝細胞で置換された肝臓を持つキメラマウスを作製した[3]．その後，筆者らも含めいくつかのグループにより，Alb-uPA/SCIDマウス[4,5]やAlb-uPA/Rag2ノックアウト[6]マウスなどが作製され，ヒト肝細胞によるマウス肝臓の置換の試みが行われた．

筆者らは他のグループに先立ち，マウス肝臓のほとんどがヒト肝細胞で置換されたキメラマウス（ヒト肝細胞キメラマウス）を安定的に生産することに成功した[4]．このマウスは，ヒト型の薬物代謝能を持つことや[4,7,8]，B型肝炎ウイルス（HBV）やC型肝炎ウイルス（HCV）に感染可能であることから[5,6]，新薬開発のための薬物代謝試験や抗HBV薬や抗HCV薬の薬効試験に使われている．

筆者らは，このヒト肝細胞キメラマウスは，*in vivo*におけるヒト肝細胞の増殖・分化能に関する研究に有用と考えている．また，ヒト肝細胞キメラマウスの肝臓では，肝細胞はヒト由来であるが，非実質細胞はマウス由来である．ヒト肝細胞キメラマウスにおけるヒト肝細胞が通常とは異なる環境におかれることにより生じる異常現象を解明することにより，肝細胞と非実質細胞，肝細胞と他組織との新たな相互作用を知りえるのではないかと考えている．本稿では，ヒト肝細胞キメラマウスで観察される異常な性質の一つである，肝重量体重比の増加について取り上げ，肝重量体重比調節メカニズムに関して考察する．

株式会社フェニックスバイオ（〒739-0046 広島県東広島市鏡山3-4-1）
Chimeric mice with humanized liver—Mechanism of hepatic hyperplasia induction—
Chise Tateno（PhoenixBio Co., Ltd., 3-4-1 Kagamiyama, Higashihiroshima, Hiroshima 739-0046, Japan）

2. ヒト肝細胞キメラマウスの作製とその利用

筆者らはAlb-uPAマウス[1]と重度免疫不全のSCIDマウスを掛け合わせたAlb-uPA/SCIDマウスを作製し[4]，現在クローズドコロニーとして株式会社フェニックスバイオにおいて系統を維持している．約3週齢のAlb-uPA/SCIDマウスに脾臓経由で米国から購入した子供のドナー由来の凍結保存ヒト肝細胞を融解後2.5〜10×10^5個注入すると，約2ヶ月でマウス肝臓の70%以上がヒト肝細胞で置換されたキメラマウスが作出できる（図1）．ヒト肝細胞を移植後，経時的にマウス血液を採取しマウス血中ヒトアルブミン濃度のモニタリングを行っている．移植後7週目（10週齢）頃まで対数的にヒトアルブミン濃度は増加するがその後安定する（図1）．マウス肝臓の7葉の組織切片を作製し，ヒト特異的サイトケラチン8/18抗体を用いて免疫染色を行い，マウス肝臓のヒト肝細胞による置換率を求めている（図2）．屠殺時のマウス血中ヒトアルブミン濃度と置換率はよく相関していることから，ヒトアルブミン濃度からマウスの置換率を推定することができる（図1）．

ヒト肝細胞キメラマウス肝臓はヒト肝臓と同等の薬物代謝酵素やトランスポーターを発現していることから[4,7,8]，新薬におけるヒト薬物代謝予測に利用されている．これまで*in vivo*でのHBVやHCVの新薬の薬効試験にはチンパンジーが使われていたが，最近では動物愛護の問題からその使用が難しくなってきている．ヒト肝細胞キメラマウスはHBVやHCVに容易に感染することができるため[5,6]，現在唯一のHBV，HCV感染小動物モデル系として利用されている．

現在，株式会社フェニックスバイオでは，移植したマウスの約8割が置換率70%以上の高置換のキメラマウスを大量生産することが可能である．年間約3,000匹のヒト肝細胞キメラマウスを生産し，これらのマウスは学術研究機関や製薬会社との共同研究や受託試験に使われている．

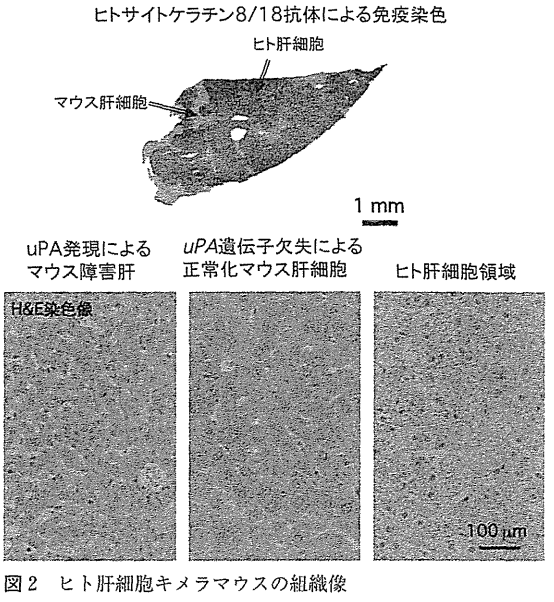

図2 ヒト肝細胞キメラマウスの組織像

3. ヒト肝細胞キメラマウスの特徴

ヒト肝細胞キメラマウス肝臓は，ヒト肝細胞とマウス由来の類洞内皮細胞，クッパー細胞，星細胞などの非実質細胞で構成されている．キメラマウス肝臓切片をヘマトキシリン・エオシン（H&E）染色すると，3種類の肝細胞が観察できる（図2）．1）uPAの発現による障害マウス肝細胞

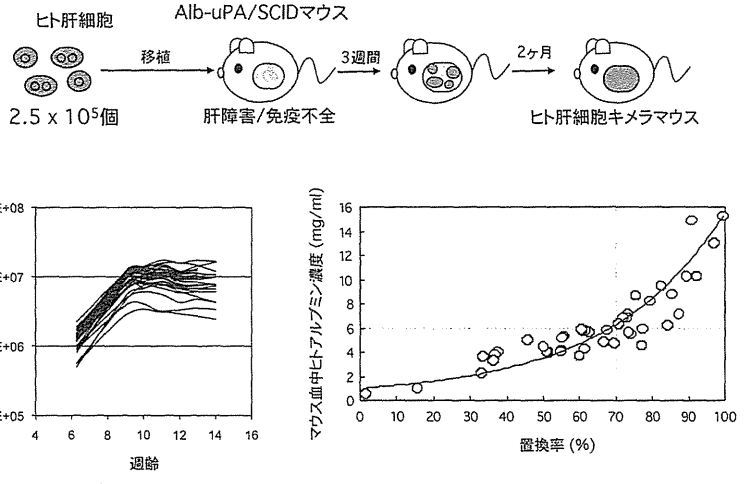

図1 ヒト肝細胞キメラマウスの作製

であり，萎縮している．細胞質に多くの小さな脂肪滴を持つ．2）肝細胞の細胞分裂の際に，導入された *uPA* 遺伝子が相同組換えにより欠失することにより正常化したマウス肝細胞である．細胞質がエオシンに好染し正常マウス肝細胞の形態を示す．3）マウス肝臓を置換したヒト肝細胞である．マウス正常肝細胞に比べて核の大きさが均一で小型であり，細胞質が淡明である．細胞質が過ヨウ素酸シッフ（PAS）染色陽性であることから，ヒト肝細胞にグリコーゲンが多く存在しているためと考えられる．これら3種の細胞の特徴は透過型電子顕微鏡でも確認できる．電子顕微鏡観察により，ヒト肝細胞領域においても，正常な類洞構造が形成されており，肝細胞と類洞内皮細胞間にはディッセ腔が存在することが確認できる．また，肝細胞間には胆汁が分泌される毛細胆管が形成されている．後に詳細に述べるが，正常なげっ歯類やヒト肝臓では，肝細胞が類洞に沿って1列に並んでいるが，ヒト肝細胞キメラマウスでは，2列に並んでいる[9]．

これらのことから，ヒト肝細胞とマウス非実質細胞はほぼ正常に構築されていると考えている．また，遺伝子発現の観点から観察すると，ヒト肝臓由来の肝細胞とヒト肝細胞由来の肝細胞の遺伝子発現をマイクロアレイで比較することにより，80～85%の遺伝子が2倍の範囲内で同等の発現をしていることを確認している．

ヒト肝細胞キメラマウスの持つ正常なヒトやマウスと異なる性質もいくつか明らかになっている．ヒト肝細胞キメラマウスは肝重量体重比が正常のマウスに比べて1.5～2.0倍高い[9]（図3）．通常，体重に対する臓器重量は動物種により決まっており，部分肝切除後も元の重量に戻る[10~12]．肝重量体重比は，マウスでは約5～6%[9]，ラットでは約3.5～4.5%[11]，ヒトでは約2～3%[12]ということが知られている．また，ヒト肝細胞キメラマウスでは血清中の胆汁酸濃度が正常マウスに比べて高いという特徴も持つ．

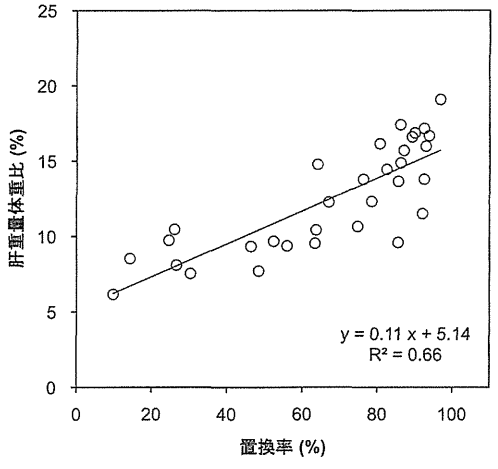

図3 ヒト肝細胞キメラマウス肝臓の肥大化

4. マウス肝細胞およびラット肝細胞キメラマウスを用いたG1からS期への移行メカニズムの探索

Weglarzらは，主要尿タンパク（major urinary protein, MUP）のプロモーターを用いたuPAトランスジェニックマウスを作製した[13]．MUPプロモーターは生後発現するという以外は，これまでのuPAマウスと同様な特徴を持つ．このMUP-uPAマウスとヌードマウスを掛け合わせ，MUP-uPA/ヌードマウスを作製した[14]．

2/3部分肝切除後のDNA合成が亢進した肝細胞の動態は，ラットとマウスで異なることが知られている．ラットでは，術後24時間と36時間に二つのピークがある．一方，マウスでは，40時間後に一つのピークがあることが知られている[14]．ラット肝細胞はマウスの体内に存在すると，どちらの動態を示すのだろうか．この疑問に答えるために，彼らは，MUP-uPA/ヌードマウスにラット肝細胞とマウス肝細胞を移植し，キメラマウスを作製した[14]．作製したラット肝細胞キメラマウスとマウス肝細胞キメラマウスに2/3肝部分切除術を施し，その後の肝細胞におけるDNA合成能をブロモデオキシウリジン（BrdU）の取り込みにより調べた．その結果，ラット肝細胞キメラマウスは，24時間と36時間，二つのピークを示し，コントロールのマウス肝細胞キメラマウスでは，マウスと同様40時間にピークを示した[14]．このことから，G1からS期への移行は，サイトカインや増殖因子による外因的な刺激よりも，内因的な性質によることが証明された．

5. ヒトおよびラット肝細胞キメラマウスの作製

筆者らは，ヒト肝細胞キメラマウスにおける肝臓の肥大メカニズムを調べるために，Alb-uPA/SCIDマウスに 7.5×10^5 個のヒト肝細胞と 5.0×10^5 個のラット肝細胞を移植し，ヒト肝細胞キメラマウスとラット肝細胞キメラマウスを作製した．移植後1週目よりマウスを安楽死させ，肝臓のサンプリングを行い肝重量体重比および置換率を求めた．さらに肝臓におけるBrdUの取り込みとタンパク質発現を免疫染色により，また，遺伝子発現を定量性リアルタイムRT-PCR法により測定した．

6. ヒトおよびラット肝細胞キメラマウスの肝重量体重比

肝重量体重比を調べると，ラット肝細胞キメラマウスは5.4%とほぼ正常マウスと同じであったが，ヒト肝細胞キメラマウスは，マウス肝臓におけるヒト肝細胞の置換率が上昇するとともに肝重量体重比が増加し，置換率約80%以上では約13%の肝重量体重比であった（図3）．また，肝臓の肥大が個々の肝細胞の肥大によるものか，肝細胞数の増加によるものかを調べるために，一定面積あたりの肝